

MODELING AND OPTIMIZING IRRADIANCE DISTRIBUTIONS IN  
AGRIVOLTAIC SYSTEMS

A Thesis

Submitted to the Faculty

of

Purdue University

by

Allison Perna

In Partial Fulfillment of the

Requirements for the Degree

of

Master of Science

December 2019

Purdue University

West Lafayette, Indiana

THE PURDUE UNIVERSITY GRADUATE SCHOOL  
STATEMENT OF COMMITTEE APPROVAL

Dr. Peter Bermel, Chair

School of Electrical and Computer Engineering

Dr. Rakesh Agrawal

Davidson School of Chemical Engineering

Dr. Muhammad Ashraful Alam

School of Electrical and Computer Engineering

Approved by:

Dr. Dimitrios Peroulis

Head of the School Graduate Program

To my grandma, for reading my thesis cover to cover  
and never asking when I'll be done.

## ACKNOWLEDGMENTS

Thank you to the entire NSF NRT SFEWS team at Purdue for their collaboration and support. Interdisciplinary work is a challenge, and I am proud to have been a part of such an effective team.

This thesis would not have been possible without the guidance of my committee members. Thank you to Professor Alam for his critical, helpful feedback during my presentations and for pushing this work to a higher caliber. I would like to extend a special thank you to Dr. Agrawal for driving this project and for his consistent guidance and support. It has been an honor to have worked with them both.

It has been a privilege to work with my advisor, Dr. Peter Bermel. Thank you to Dr. Bermel for valuable discussions on the technical direction of my work, and for keeping me from drowning in the details. I have learned and grown significantly under his mentorship during my time at Purdue, both technically and professionally. For this I am grateful.

I would like to give a personal thank you to the Purdue Counseling and Psychological Services center for their compassionate care. They are the unsung heroes of this work.

Lastly, to my family and dear friends, thank you. I would not be who I am or have achieved this degree without their unconditional love and support.

## TABLE OF CONTENTS

	Page
LIST OF TABLES . . . . .	vii
LIST OF FIGURES . . . . .	viii
ABBREVIATIONS . . . . .	x
ABSTRACT . . . . .	xi
1 INTRODUCTION . . . . .	1
1.1 Co-production of Agriculture and Electricity . . . . .	1
1.1.1 Agrivoltaics . . . . .	2
1.1.2 APV System Metrics . . . . .	3
1.1.3 Proposed and Existing Systems . . . . .	4
1.2 Modeling Agrivoltaic Systems . . . . .	5
1.2.1 PV System Modeling . . . . .	6
1.2.2 Agricultural System Modeling . . . . .	8
1.2.3 Analytical Models . . . . .	8
1.3 Design Considerations . . . . .	8
1.3.1 Crop Needs . . . . .	9
1.3.2 Photovoltaic System . . . . .	10
1.4 Overview of this work . . . . .	10
2 MODELING SHADOW PATTERNS IN AGRIVOLTAIC FARMS . . . . .	12
2.1 Models . . . . .	12
2.1.1 Irradiance Model . . . . .	14
2.1.2 Shadow Position Algorithm . . . . .	15
2.1.3 Error . . . . .	18
2.1.4 Electrical Power Model . . . . .	20
2.1.5 Code Availability and nanoHUB Tool . . . . .	22

	Page
2.2 Estimating Crop Yield . . . . .	22
3 DESIGNING OPTIMIZED AGRIVOLTAIC STRUCTURES FOR COPRO- DUCTION OF SOLAR ENERGY AND CROP BIOMASS . . . . .	23
3.1 Effects of PV System Configuration . . . . .	23
3.1.1 Case study: ACRE Farm . . . . .	25
3.2 Row Width, Panel Width . . . . .	27
3.3 Panel Patterning . . . . .	30
3.3.1 Checkerboard Pattern . . . . .	34
3.3.2 Parallel Stripes . . . . .	39
3.4 Summary and conclusions . . . . .	41
4 TRACKING ALGORITHMS TO MANIPULATE SHADOWS . . . . .	43
4.1 AOI Manipulation . . . . .	44
4.2 Summary . . . . .	45
5 SUMMARY, RECOMMENDATIONS, AND FUTURE WORK . . . . .	47
5.1 Summary and Recommendations . . . . .	47
5.1.1 Updates to Model . . . . .	48
5.1.2 Bifacial PV . . . . .	48
5.1.3 Spectrally-Selective PV Systems . . . . .	49
5.1.4 Advanced Tracking . . . . .	49
REFERENCES . . . . .	51

## LIST OF TABLES

Table	Page
1.1 Existing Commercial Agrivoltaic Systems (Adapted from [10]) . . . . .	6
1.2 Existing Research Agrivoltaic Systems (Adapted from [10]) . . . . .	7
2.1 Device IV Characteristics for Electrical Power Model . . . . .	21
3.1 Parameters and metrics for systems in Fig. 3.1 and related [3]. . . . .	25
3.2 PV effects on insolation for different locations and diffuse indices. . . . .	25
3.3 Purdue ACRE Agrivoltaic System Parameters. . . . .	26
3.4 Tracking Parameters for data set in Fig. 3.6, Fig. 3.7, Fig. 3.8, and Fig. 3.9.	30
3.5 Input parameters for parallel and perpendicular stripes data sets in Fig. 3.7, Fig. 3.6, Fig. 3.8, and Fig. 3.9. The same panel dimensions are used for both systems. Length is varied to ensure proper infinite periodicity of each pattern, not affecting results that are per unit area. . . . .	34
3.6 Checkerboard Shadow Effects. Spatial average and standard deviation in shadow depth. Spatially average maximum shadow duration in time for midday and full day [30]. . . . .	39

## LIST OF FIGURES

Figure	Page	
2.1	Flowchart of simulation framework. . . . .	13
2.2	Examples of Irradiance Models. . . . .	15
2.3	Percent error in calculated shadow dimension for various panel dimensions and elevation from ground (height). This is for the case of the sun at the zenith point above a horizontal panel. . . . .	18
2.4	Maximum panel dimensions to eliminate shadows. . . . .	19
3.1	Shadow depth of different configurations in West Lafayette, IN. [30]. PV system parameters in Table 3.1. Case E utilizes checkerboard patterning elaborated on in section 3.3. . . . .	24
3.2	Direct shadow depth spatial maps at Purdue ACRE farm for four months of the growing season: a) May 1, 2019, b) June 1, 2018, c) July 1, 2018, and d) August 1, 2018. Photovoltaic panels are displayed in semi-transparent gray at 0°tilt from the horizontal. . . . .	27
3.3	Effect of row width on shadow depth. . . . .	28
3.4	Effect of panel width on shadow depth. . . . .	29
3.5	Panel patterns. . . . .	30
3.6	Pareto front visualization of shadow depth average vs. spatial power density, simulated for June 1, 2018. Shadow depth from GHI given in (a-c); shadow depth from direct horizontal irradiance only given in (d-f) for California ( $k_d=0.19$ ), Texas ( $k_d=0.31$ ), and Indiana ( $k_d=0.41$ ) locations. Checkerboard (CB), perpendicular (perp.) and parallel (par.) patterns shown. . . . .	32
3.7	Pareto front visualization of shadow depth homogeneity (spatial standard deviation) vs. spatial power density, simulated for June 1, 2018. Shadow depth from GHI given in (a-c); shadow depth from direct horizontal irradiance only given in (d-f) for California ( $k_d=0.19$ ), Texas ( $k_d=0.31$ ), and Indiana ( $k_d=0.41$ ) locations. Checkerboard (CB), perpendicular (perp.) and parallel (par.) patterns shown. . . . .	33

Figure	Page
3.8 Pareto front visualization of spatially averaged maximal shadow duration for each field finite element from sunrise to sunset vs. spatial power density, simulated for June 1, 2018. Standard deviation of this spatial average shown in (D-F). Minimal shadow duration and maximal power production are desired for optimal APV system performance. Checkerboard (CB), perpendicular (perp.) and parallel (par.) patterns shown. . . . .	35
3.9 Pareto front visualization of spatially averaged maximal shadow duration for each field finite element from 10 a.m. to 4 p.m. local time vs. spatial power density, simulated for June 1, 2018. Standard deviation of this spatial average shown in (D-F). Minimal shadow duration and maximal power production are desired for optimal APV system performance. Checkerboard (CB), perpendicular (perp.) and parallel (par.) patterns shown. . . . .	36
3.10 Effect of checkerboard dimensions on shadow depth [30]. . . . .	37
3.11 Effect of checkerboard dimensions on shadow depth [30]. . . . .	38
3.12 Effect of checkerboard dimensions on shadow duration [30]. Time-series data for the California location on June 1, 2018. Black indicates direct shadow. Checkerboard dimensions are 0.15m x 0.15m and 0.3m x 0.3m and the same PV area is used (1.5m width vs. 3m width for 50% PV density checkerboard). . . . .	40
3.13 Homogeneity of parallel stripes vs. row width. Each color is a different data set from Table 3.5. The minima correspond to the 7 m row width for the Indiana location on June 1, 2018. . . . .	41
4.1 Coordinate system for Eqn. 4.6 . . . . .	46
4.2 Definition of AOI. . . . .	46

## ABBREVIATIONS

APV	Agri-Photovoltaic, agrivoltaic, agrophotovoltaic
PV	Photovoltaic
SD	Shadow Depth
N	North
S	South
E	East
W	West

## ABSTRACT

Perna, Allison M.S., Purdue University, December 2019. Modeling and Optimizing Irradiance Distributions in Agrivoltaic Systems. Major Professor: Peter Bermel.

Land use constraints have motivated investigation into the spatial coexistence of solar photovoltaic electricity production and agricultural production. Previous work suggests that agriculture-photovoltaic (agrivoltaic) systems either decrease crop yield or are limited to shade-tolerant crops. Existing experimental work has also emphasized fixed south-facing configurations with traditional commercial panel shapes, and modeling work is sparse. In this work, the effects of different photovoltaic array configurations and panel designs on field insolation spatial and temporal variation are explored in detail to determine photovoltaic design routes that may increase expected crop yield in agrivoltaic systems. It is found that photovoltaic row orientation is the most influential factor on insolation homogeneity due to shadow migration paths. Additionally, it is shown that utilization of mini-modules in patterned panel designs may create more optimal conditions for plant growth while using the same area of PV, thus improving the land efficiency ratio of the agrivoltaic system. Different solar tracking algorithms are explored to optimize the trade-off between electricity production and expected crop growth. The feasibility of select agrivoltaic systems is explored for multiple U.S. locations. This thesis concludes with recommendations for photovoltaic system designs corresponding with specific crop growth considerations.

## 1. INTRODUCTION

The global population is expected to increase to nearly 10 billion by 2050 [1]. With this population increase, a substantial rise in food and energy demands is anticipated. Additionally, increasing desires to mitigate climate risks and improve energy independence are pushing humanity to shift to carbon-free forms of energy production. In this renewable energy shift, wind and solar are expected to dominate the renewable energy landscape [2]. However, these are two highly land-intensive technologies in terms of land area required for equivalent net electricity compared to fossil fuels [3]. Utility scale PV parks in the U.S. generate 4-11  $\text{W m}^{-2}$  of land with a national average of 7  $\text{W m}^{-2}$  [3, 4]. Power spatial density is even lower for wind farms, which typically generate 1-3  $\text{W m}^{-2}$  [3].

Increased deployment of land-intensive energy technologies paired with increased food demand creates a competition for land, potentially threatening current agriculture. Recent work has demonstrated that there is insufficient land for widespread PV or wind deployment in a 100% renewable energy economy by taking into account the complexities of land use constraints. This suggests that novel systems need to be utilized to overcome land use constraints of deploying photovoltaic systems as the primary energy source in the U.S. [3]. Even without a goal of 100% renewable energy, similar competition for land resources exists in densely populated regions with high energy demand and in regions with significant land that's unsuitable for PV [5].

### 1.1 Co-production of Agriculture and Electricity

To address this competition in a sustainable and renewable fashion, systems achieving sustainable co-production of energy and food on the same land area have been proposed [3, 5, 6]. In these co-production systems, electricity generation can take

the form of photovoltaic arrays, wind farms, or utilization of plants for biofuel [3, 7]. Wind resources are often utilized for food and energy co-production purposes with wind turbines occupying the same land as agricultural activity (crop or pasture), however, wind resources are regionally limited and wind turbine spatial power density is smaller than that of commercial photovoltaic arrays [3]. Biofuel co-production is also unlikely to be viable [7]. Since the solar resource is available year-round for the majority of agricultural regions [8, 9], it is likely that a synergistic approach between the dominant renewable energy technologies (wind and solar) and agricultural land production is both promising and necessary to comprehensively address land constraints as society strives to meet future food and energy demands [3].

### 1.1.1 Agrivoltaics

Agrivoltaic or agrophotovoltaic (APV) systems combine agricultural production and renewable solar photovoltaic energy production on the same land area. In contrast to common ground-mounted PV arrays, APV systems are elevated by multiple meters to allow for movement of agricultural equipment or to allow room for grazing animals [10]. In addition, APV systems often have wider spacing between photovoltaic rows than their energy-oriented PV field counterparts to allow for increased irradiance available to the crops growing below the PV array [11–13]. Though it is expected and often observed that crop yield diminishes with decreased irradiance [14], agrivoltaic systems have the potential to improve agricultural production. When irradiance levels are detrimentally high, photovoltaic panels can provide shading that improves crop yield. This has been achieved by Fraunhofer ISE in 2018 during an exceptionally hot summer [12]. By decreasing the radiation reaching crops by roughly 30% via an APV system, potato and winter wheat yields increased by 3% each and celery yield increased by 12% compared to the reference plot [12]. Controlled tracking can mitigate this irradiance reduction, as demonstrated in France by Valle [15]. Additionally, there is potential for controlled tracking to optimize field irradiance for

heat and light sensitive crops [16], offering potential as a resource-efficient sustainable system [10]. Because of this potential for irradiance control, agrivoltaic systems have high potential for synergistic effects in semi-arid and arid regions with excessively high irradiance such that the reduced irradiance mitigates light and heat stress and water loss experienced by crops [10, 17].

### 1.1.2 APV System Metrics

There are two major schools of thought within the agrivoltaic community on how to achieve sustainable food and energy co-production. The most common argument is an increase in overall land productivity, typically at the cost of both agricultural and electricity production when comparing net production of the agrivoltaic system to expected production on the same land area with single-use, either photovoltaic or agriculture.

To quantitatively describe this increase in land productivity, the similar metrics “Land Use Efficiency” [11, 12] and “Land Equivalent Ratio” (LER) [7] have been recently adopted. LER is used to assess the productivity of mixed systems by comparing the land required to achieve the productivity of the mixed system to the land equivalent to achieve the same productivity in single-use systems, such as intercropping compared to monocrop systems [7]. Land use efficiency is defined similarly but emphasizes the increase in production on the same land by implementing a dual-use strategy. LER of any aglectric system is defined as:

$$LER = \frac{Y_{crop, aglectric}}{Y_{crops \ only}} + \frac{Y_{electricity, aglectric}}{Y_{electricity \ only}} \quad (1.1)$$

For the agrivoltaic system,  $Y_{crop, aglectric}$  is the crop yield in the agrivoltaic system,  $Y_{crops \ only}$  is the crop yield expected from a monocrop agricultural system on the same land area,  $Y_{electricity, aglectric}$  is the electricity yield from PV in the agrivoltaic system, and  $Y_{electricity \ only}$  is the electricity yield for the PV system that would have

utilized the same land area. Reference plots for PV and for agriculture are often used in conjunction with experimental APV systems to determine appropriate values for  $Y_{crops\ only}$  and  $Y_{electricity\ only}$ .

Fraunhofer ISE has demonstrated 186% land use efficiency in an APV system growing potatoes [12]. Dupraz (2011) has modeled LER values of 1.73 and 1.35 for their full density (1.6 m PV row spacing) and half density (3.2 m PV row spacing) systems, respectively. These systems were modeled to experience a 27% (full density) and a 17% (half density) reduction in crop yield. Weselek (2019) reviewed existing APV technology, concluding that APV can increase overall land productivity by 70% [10].

Another approach that has more recently gained traction is the idea of designing the PV system for agriculture such that zero crop loss is experienced [3, 10]. In this realm, the term ‘aglectric’ is used, referring to systems with vertical development of land to include electricity production without reducing net agricultural output, thereby improving overall land productivity per unit area and ultimately maintaining global food supply [3].

### 1.1.3 Proposed and Existing Systems

The first agrivoltaic paper was published by Goetzberger and Zastrow in 1982 [6]. This foundational work proposed an analytical model that estimates radiation distributions on the ground below south-facing elevated PV arrays, laying the groundwork for the agrivoltaic field. Goetzberger founded Fraunhofer Institute for Solar Energy Systems ISE in 1981. Decades later, Fraunhofer ISE published work on their first agrivoltaic systems using the fixed-tilt south-facing elevated array design proposed by Goetzberger [6, 11, 12].

In the past decade, some theorized agrivoltaic systems have been implemented in Europe with varying success [11–13, 15, 18]. These are divided into commercial systems (Table 1.1) and research systems (Table 1.2). All commercial APV systems

examined in [10] utilize solar tracking, while research APV systems vary in their use of tracking. All systems, commercial and research, use existing PV panel technology, instead varying array-level parameters such as the row spacing between panels to increase irradiance available to crops [13]. Solar tracking algorithms are implemented to either mitigate adverse effects on crops from irradiance loss during key hours of the day [15] or to increase electricity production [18]. All systems are elevated, as well, varying between about 3 and 5 m [10].

Most existing APV systems cultivate minor commercial crops, frequently focusing on shade-tolerant plants that are likely to still thrive under low irradiance conditions such as lettuce and potatoes [7, 11–13]. The common approach is fitting the crop to the PV system, and a significant number of studies in the agrivoltaic field to date have been conducted agronomy specialists. Some APV technology seeks to design the PV system for crop growth, however, focusing on novel panel designs, both geometric and spectrally selective, and on novel tracking algorithms to optimize the trade-off between crop yield and electricity production [3, 15, 18].

## 1.2 Modeling Agrivoltaic Systems

APV systems have many different factors influencing their overall functioning, requiring the combination of multiple separate models of varying complexity to understand [10]. To this end, irradiance distribution models, PV electricity yield models, crop models, and microclimate models are all utilized [10]. It is well-known in the literature and the PV community how to model anticipated electricity yield from a given PV system. However, PV system impact on agronomic aspects of the APV system is not well-understood nor thoroughly explored, giving crop models an important purpose in understanding the possible effects on crop growth [10].

Table 1.1.: Existing Commercial Agrivoltaic Systems (Adapted from [10])

Ref.	Site, Country	Capacity ( $kWp$ )	Solar Tracking	Cultivated Crops
[19, 20]	Monticelli D'Ongina, Italy	3230	Dual-axis	Winter wheat, maize
[19, 20]	Castelvetro, Italy	1294	Yes	Winter wheat, maize
[19, 20]	Virgilio, Italy	2150	Yes	Winter wheat, maize
[21]	Abruzzo, Italy	800	Yes	Pasture, tomato, watermelon, wheat
[20]	Anhui province, China	544	Yes	Unknown
[22]	Zhejiang province, China	544	Yes	Rice

### 1.2.1 PV System Modeling

Photovoltaic systems can be modeled with various levels of complexity. To estimate power capacity of a given system, the single-diode model can be used [23]. This model, however, does not take into account system level losses, such as mutual PV row shadowing that causes mismatch losses [24]. More complex models take into account module and array level losses, which can also be characterized by a single metric, the performance ratio. The performance ratio for photovoltaics is an internationally established metric for measuring PV system performance loss from less light utilization, temperature variation, and various system-level losses and failures [25, 26].

Table 1.2.: Existing Research Agrivoltaic Systems (Adapted from [10])

Ref.	Site, Country	Capacity ( <i>kWp</i> )	Solar Tracking	PV System Di- mensions	Cultivated Crops
[16]	Arizona, USA	Unknown	No	Cabbage, chard, kale, tomato, onion	
[13, 15]	Montpellier, France	Unknown	Fixed-tilt (25° tilt, 11° E of S) and E-W tracking (standard and con- trolled)	Fixed: 0.8-m wide panels, 22.4-m long rows, 4-m height, 1.6-m and 3.2-m row spacing; Track- ing: 1.98-m wide panels, 5-m height, 19-m long rows	Cucumber, durum wheat, French bean, lettuce
[10]	Heggelbach, Germany	194	Fixed-tilt	–	Winter wheat, clover grass, celeriac, potato
[27, 28]	(Fraunhofer Chile Research) Santiago de Chile, Chile	Unknown	Fixed-tilt	13-m row length, 8 rows 2.5-m PV row spacing	Various cabbage varieties (broccoli, cauliflower, kale), potato, pumpkin
[10]	Chiba Prefec- ture, Japan	Unknown	Fixed-tilt	750-m <sup>2</sup> and 7.7 acres farmland, 3- m and 5-m height, row spacing 5-m, panels separated along row length	Cabbage, cucum- ber, eggplant, peanut, tomato, taro, yam

### 1.2.2 Agricultural System Modeling

The effects that APV has on microclimate have not been thoroughly explored in either experimental or modeling literature [10, 14]. At the time of writing, this is a goal of the InSPIRE project at the National Renewable Energy Laboratory in Golden, CO [29]. The potential of APV systems for specific crops has been explored using a combination of models [5, 7]. These studies have focused on existing PV technology. Recently modeling work has demonstrated irradiance distributions at the crop level for certain existing and novel APV system designs [3, 30].

### 1.2.3 Analytical Models

Goetzberger and Zastrow [6] developed the first analytical models for south-facing fixed tilt agrivoltaic systems in the 1980s. Their analytical model assumed i) a south-facing array infinite in x and y directions, ii) the mounting structure does not contribute to shadowing, iii) the PV panels are ideal absorbers, iv) an isotropic diffuse sky model, and v) direct radiation integrated over daylight hours will be spatially uniform in x and y for sufficient panel height. They developed a trigonometry-based analytical model and used it to calculate spatial radiation distributions for two example PV configurations, finding an insignificant variation in diffuse light for the isotropic sky case. However, assumption (v) on uniform diffuse light is incorrect. This is elaborated upon in Chapter 2. This thesis proposes corrections to the model and complex simulation work to account for the true spatial variation of direct light.

## 1.3 Design Considerations

To design high performing agrivoltaic systems, one must understand the effects that irradiance levels and different shading conditions can have on crop biomass and quality [10]. For photovoltaic panels, it is worth discussing both the design parameters

for PV systems that are specially-designed for APV, existing photovoltaic panels available off-the-shelf, and common practices in PV array installation.

### 1.3.1 Crop Needs

Whether one is designing a PV system for APV applications, choosing a suitable crop for a given APV system, or optimizing an APV system with both approaches, crop irradiance and other microclimate needs must be strongly considered. Major agricultural crops in the U.S. generally undergo one of two major photosynthesis types: C3 or C4. As distinct metabolic pathways, they experience different utilization of resources such as water, CO<sub>2</sub>, and photosynthetically active radiation (PAR). In the case of C3 plants, the photosynthetic rate generally saturates at lower levels of irradiance (i.e. photosynthetic saturation irradiance,  $I_{sat}$ ). This behavior suggests that redirecting the irradiance of crops for electricity production may not affect crop yield, which is corroborated by our collaborators at Purdues Department of Agronomy [31], as well as a recent review paper on APV crop yields [10]. Cotton and rice, two major crops, have saturation irradiance values of approximately 1300  $\mu\text{mol m}^{-2} \text{s}^{-1}$  of photosynthetically active radiation [33, 34], which corresponds to GHI values of approximately 650  $\text{W m}^{-2}$  of the full AM1.5G spectrum, which is significantly lower than the average midday irradiance for many warm major agricultural regions during the summer growing season [8, 32], suggesting redirection of part of the solar spectrum in these regions may not greatly negatively affect net crop yield. It is also well established that other factors such as water availability in non-irrigated agricultural fields oftentimes provide more of a constraint on crop growth than irradiation availability.

Still, there are multiple requirements associated with sunlight to maintain crop yield. For field crops, homogeneity of irradiance reductions is crucial for most single-crop farming practices. Additionally, the duration of direct shadows during periods of low irradiance (near sunrise and sunset) may push plants into low photosynthetic rate

regimes, or possibly into respiratory regimes, which can negatively impact plants [31]. There is limited literature on the effects of shading on plant characteristics due to the complexity of crop growth, type of shading conditions, and the plethora of plant attributes [10]. Literature on shading effects was recently compiled [10] showing that a variety of negative and positive effects on plant yield and quality are observed, depending on the plant and the shading condition. Since changes in microclimate beyond shading in APV systems can affect crop yield [13], it is suggested that there is a strong need for studies on crop cultivation in APV systems [10].

### **1.3.2 Photovoltaic System**

The design of the photovoltaic system component of APV systems is instrumental to the APV system productivity. PV installation methods are typically high-impact on the land. Furthermore, APV systems may require heavy machinery for installation of physically-stable elevated structures that support the weight of off-the-shelf PV modules. Low-impact PV installation can support the existing and continued utilization of land for agriculture [29]. Current PV installation practices utilize heavy machinery that can damage the existing landscape. They are typically low to the ground. APV systems, however, are highly elevated thus requiring specialized installation.

Photovoltaic panels available commercially are typically large at 65” by 39” for 60-cell residential panels and 78” by 39” for 72-cell commercial panels and weighing 31-44 lbs [35]. ‘Mini modules’ have potential in APV systems that utilize patterning, as is suggested by this thesis.

## **1.4 Overview of this work**

For this work, we sought to investigate how different photovoltaic panel patterns and system configurations affect irradiance distributions on the field. Studies of the crop-level microclimate in an agrivoltaic system showed that crop-level irradiance is

the most impacted microclimate factor in an agrivoltaic system compared to typical agricultural fields [14].

The shadowing effects in both small-scale experimental agrivoltaic farms and large commercial farms are important for the field of agrivoltaics. Furthermore, variation along the panel length and width for certain proposed panel patterns [3] required the development of a 3-dimensional model comprehensive enough to capture shadowing effects caused by these 2-dimensional patterns that vary in both areal directions. To this end, a non-periodic mode to capture edge effects and an infinite periodicity mode were developed to simulate a broad range of realistic systems. Both modes represent the ground as an  $M \times N$  finite element matrix. Further details of this model and the corresponding simulation framework are described in Chapter 2.

Using this model, shadowing effects of PV systems in agrivoltaic farms were modeled. Based on this initial understanding of the interplay between diurnal solar motion, irradiance composition and intensity, and PV system array configuration, the trade-off between solar power capacity and expected crop biomass is quantified and maximized in Chapter 3, using Pareto front optimization. In Chapter 4, an early study of tracking algorithms that minimize shadowing is conducted for APV systems requiring high irradiance levels on the field for specific times of day or months of the year. We conclude this work by proposing system designs that most effectively account for different crop needs to maximize biomass and electricity output, and by outlining potential paths to enhance the performance of APV systems.

## 2. MODELING SHADOW PATTERNS IN AGRIVOLTAIC FARMS

### 2.1 Models

The model functionally flows as described in Fig. 2.1. We define a physical description of the panel system, which includes the panel pattern and dimensions, tracking or fixed-tilt with corresponding specifics, and electrical properties for calculating power capacity. We also define PV system properties such as row width, number of panels for the non-periodic mode, and period dimension (north-south and east-west) for the infinite periodicity mode. Environment parameters are defined, including latitude, longitude, altitude, and various irradiance parameters. For the simulations in this thesis we imported environmental data from NASA [32] (see Irradiance Model section for details). Lastly, the simulation time frame is defined. Though any time frame can be supported, simulations in this thesis calculate outputs on a daily basis or show the time variation of an output.

Internally, the program then develops a daily irradiance model including solar position using Sandia’s Solar Positioning Algorithm (SPA) as implemented by PVLlib [36,37] for all time steps. A time resolution of 1 minute was chosen for all simulations in this thesis unless otherwise noted to capture diurnal shadow migration with high accuracy. Next, the program determines tracker angle and panel position based on the daily solar position model. Using the irradiance model and panel position as a function of time, shadow positions are mathematically calculated for each time step and the shadowed area is recorded in the finite square element matrix using a line-drawing algorithm implemented by MATLAB [38]. Direct and diffuse radiation is integrated for each finite element, and temporal variation in direct and diffuse radiation is calculated for select points in the plot.

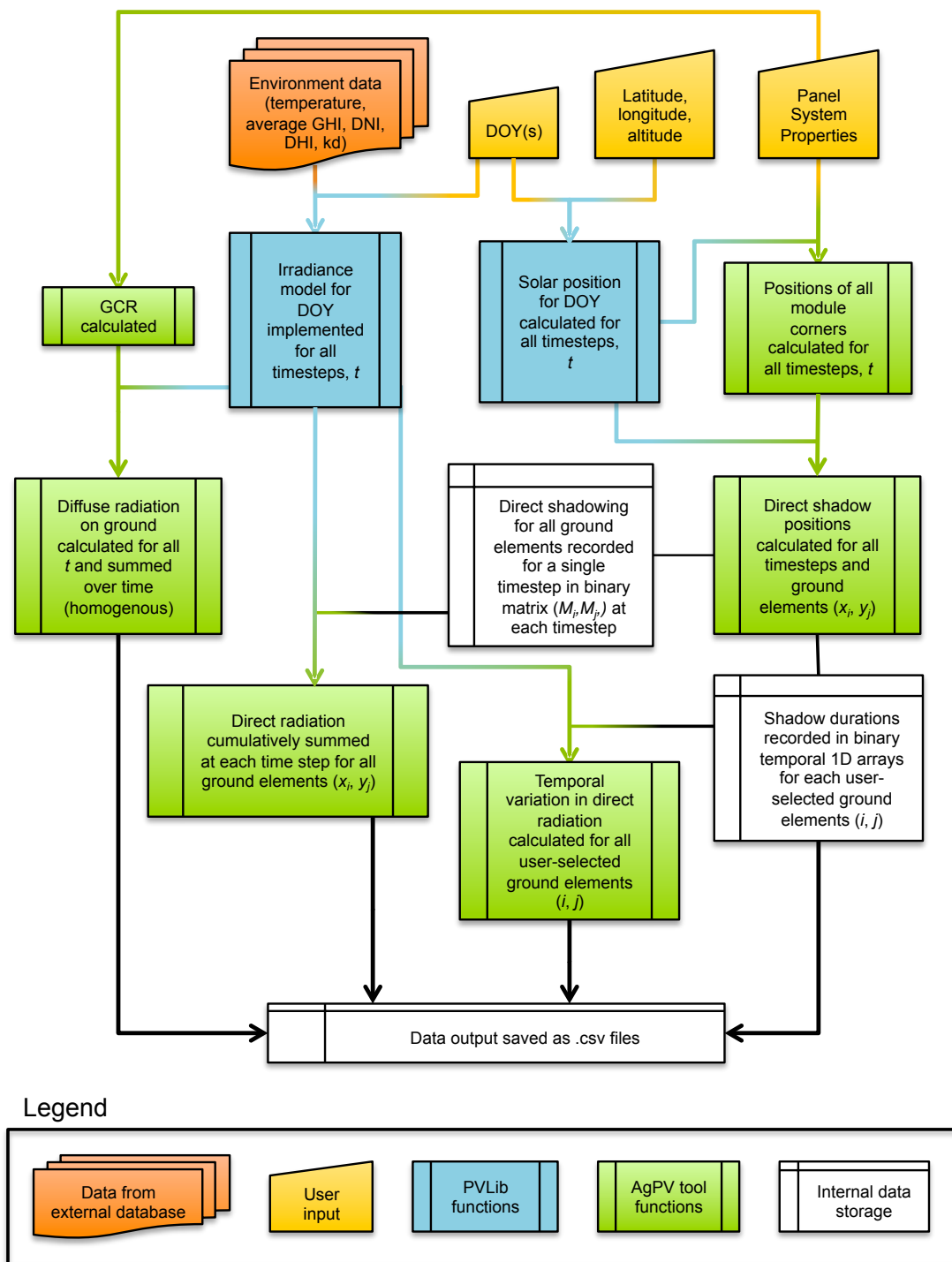


Fig. 2.1.: Flowchart of simulation framework.

### 2.1.1 Irradiance Model

PVLib is used to implement the solar positioning algorithm (SPA) using 22-year averaged monthly temperature data from NASA [32, 37]. The Haurwitz clear sky model is used to generate GHI, which is then normalized by 22-year averaged monthly global horizontal irradiance (GHI) from NASA using the apparent solar zenith angle [32].

$$GHI(t) = GHI_{Haurwitz}(t) \left[ \frac{GHI_{NASA}}{\text{mean}(GHI_{Haurwitz}(t))} \right] \quad (2.1)$$

GHI is then decomposed into the diffuse and direct components using the Orgill and Hollands model [40]. Fig. 2.2 shows the resulting irradiance model for a low diffuse light region (Fig. 2.2 (a), Fresno, CA) and a high diffuse light region (Fig. 2.2 (b), West Lafayette, IN). The correction from normalization is not significant for sunny California where the clear sky assumption is close to reality, but this correction from the clear sky model is necessary in frequently overcast regions such as Indiana.

Having an accurate diffuse to direct ratio is critical for this agrivoltaic model because diffuse and direct light are treated differently. It is assumed that 100% of direct light does not reach area on the ground that is in direct shadow. We refer to this assumption 'binary direct shadowing' to indicate that direct light is 100% or 0% included at each ground element depending on the direct shadowing. See section 2.1.3 for details on error introduced by this assumption. It is also assumed that, due to the high elevation of panels simulated in this work (5 m) that all diffuse light that is not incident on the panels reaches the ground uniformly. Error introduced by this assumption is assumed to be negligible and is not calculated in this work. The fraction of incident light on the panels is determined by the Perez model as implemented by PVLib [36, 39], which is subtracted from the total diffuse irradiance at each time step then distributed on the ground to maintain energy conservation.

$$DHI_{ground}(t) = DHI_{tot}(t) - DHI_{PV}(t) \quad (2.2)$$

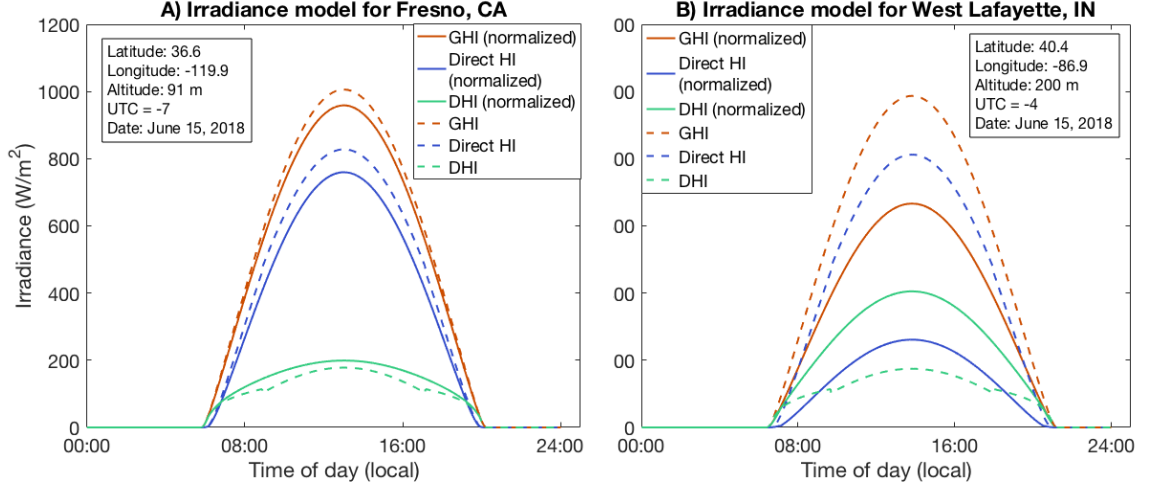


Fig. 2.2.: Examples of Irradiance Models.

### 2.1.2 Shadow Position Algorithm

The program uses a finite element mesh of  $M \times N$  elements to represent the flat ground. Each element is square with dimensions  $0.001 \text{ m} \times 0.001 \text{ m}$  (unless otherwise specified). The ground is not patterned and the elevation is at  $0 \text{ m}$  (unless otherwise specified).

The physical location of shadows is determined mathematically at each time step by mapping rays from each opaque panel segment to the ground modeling the sun as a plane source. Noting the angular diameter of the sun is  $0.53^\circ$ , this assumption is reasonable for larger panel sizes and lower panel elevations from the ground. However, this work presents shadow dimension and intensity data for certain combinations of panel dimensions and elevations that may be significantly different from reality.

Using the solar elevation angle ( $\theta_{el}$ ), solar azimuth angle ( $\psi_{az}$ ), and coordinate positions ( $x_c, y_c, z_c$ ) of each corner of each opaque panel segment, shadow positions are

mathematically determined. Solar azimuth angle is shifted to Cartesian coordinate system with +x axis as South and 0, +y axis as East and 90, and +z axis towards the Zenith.  $\psi_{az}$  will hereby be assumed to be the solar azimuth angle with respect to this coordinate system for the remainder of the thesis.

$$x_{shadow} = \frac{z_c}{\tan \theta_{el}} \cos(\psi_{az} + 180) + x_c \quad (2.3)$$

$$y_{shadow} = \frac{z_c}{\tan \theta_{el}} \sin(\psi_{az} + 180) + y_c \quad (2.4)$$

These absolute points in physical space are inputed to the MATLAB function `poly2mask.m`, which connects the four points in the finite element mesh using a line drawing algorithm for grids [38]. It converts all covered points,  $s(i, j)$ , to 'false' from 'true' to indicate direct shadow. The resulting mesh is multiplied by direct irradiance normal to the ground ( $I_{dir}(t)$ ), the fraction of diffuse light incident on the ground (Eqn. 2.5) is added, and net energy incident on each element of area  $\Delta A$ ,  $E(i, j, t)$ , over each timestep, is determined. It is assumed that zero irradiance is available before sunrise and after sunset.

$$I_{dif,g} = I_{dif}(1 - f_{PV}(t)), \quad (2.5)$$

where  $f_{PV}(t)$  is the fraction of diffuse light incident on the panel using a diffuse light model such as Perez or isotropic sky.

$$E(i, j)_{g,dir} = \sum_{t=sunrise}^{t=sunset} s(i, j, t) I_{dir}(t) \Delta t \Delta A \quad (2.6)$$

$$E(i, j)_{g,dif} = \sum_{t=sunrise}^{t=sunset} I_{dif,g}(t) \Delta t \Delta A \quad (2.7)$$

$$E(i, j)_g = E(i, j)_{g,dir} + E(i, j)_{g,dif} \quad (2.8)$$

The total reference incident energy for a given day of year on the ground is similarly calculated for an open-field system (no PV):

$$E(i, j)_{ref,dir} = \sum_{t=sunrise}^{t=sunset} I_{dir}(t)\Delta t\Delta A \quad (2.9)$$

$$E(i, j)_{ref,dif} = \sum_{t=sunrise}^{t=sunset} I_{dif,g}(t)\Delta t\Delta A \quad (2.10)$$

$$E(i, j)_{ref} = E(i, j)_{ref,dir} + E(i, j)_{ref,dif} \quad (2.11)$$

To compare the effect that PV in agrivoltaic systems has on irradiance across systems, we developed a metric called 'shadow depth.' Shadow depth (SD) is the percent reduction in incident solar energy on a given area of land over a given period of time. This metric eliminates dependence on the absolute value of GHI for a given day. Radiation spatial distribution is then dependent on the fraction of direct vs. diffuse irradiance, and on solar diurnal migration, which is a function of latitude, longitude, and day of year. For this thesis, shadow depth refers to energy integration from sunrise to sunset for a given day of year unless otherwise noted. As a function of position, it is given by:

$$SD(i, j) = 100\% * \left[ \frac{E(i, j)_g + E(i, j)_{ref}}{E(i, j)_{ref}} \right] \quad (2.12)$$

Shadow depth can also be defined in terms of diffuse fraction,  $k_d(t)$ :

$$I_{GHI}(t) = I_{dif}(t) + I_{dir}(t) \quad (2.13)$$

$$I_{dif}(t) = k_d(t)I_{GHI}(t) \quad (2.14)$$

$$SD(t) = I_{GHI}(t) [(1 - k_d(t))A_{sun}(t) + k_d(1 - f_{PV}(t))] \quad (2.15)$$

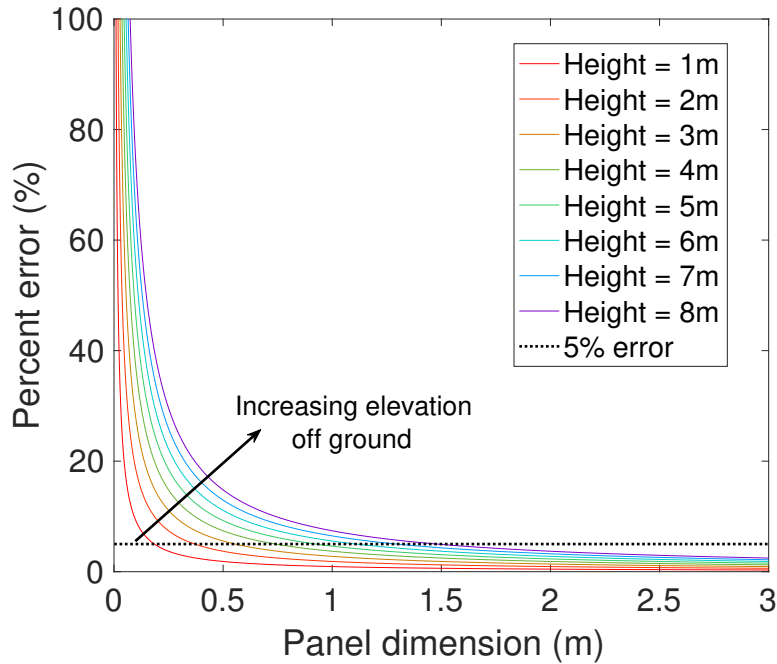


Fig. 2.3.: Percent error in calculated shadow dimension for various panel dimensions and elevation from ground (height). This is for the case of the sun at the zenith point above a horizontal panel.

### 2.1.3 Error

Fig. 2.3 shows the percent error in calculated shadow dimension for a flat panel case with the sun at zenith. This plot compares calculated shadow size from modeling the sun as a plane source to the calculated shadow size from modeling the sun as a point source with  $0.53^\circ$  angular spread. The plane source model overestimates shadow dimension with greater error for small panel dimension and high panel elevation. However, we keep the assumption of modeling the sun as a plane source because of the simplicity and because this introduced error causes our results to be more detrimental than expected in reality.

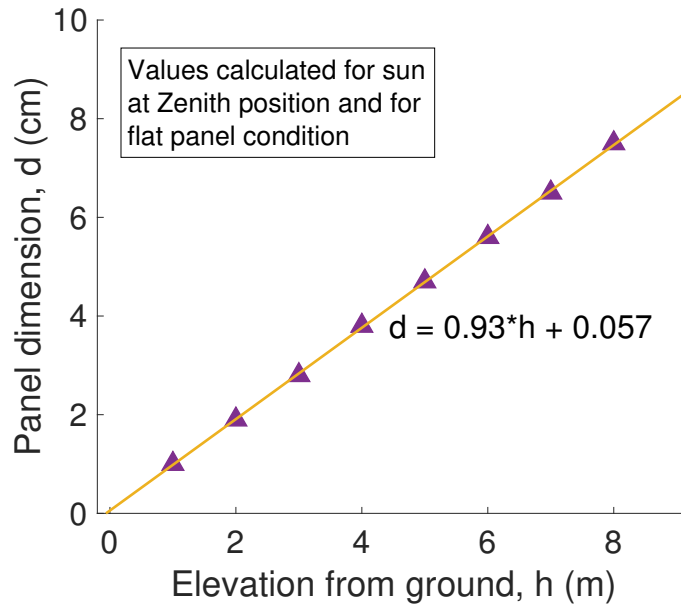


Fig. 2.4.: Maximum panel dimensions to eliminate shadows.

Fig. 2.4 shows the minimum panel dimension to eliminate shadows for various panel distances from the ground. These values are calculated for the flat panel case ( $0^\circ$  tilt to the horizontal) and with the sun directly overhead at the Zenith. We find that very small panel dimensions are required to effectively eliminate full shadows, approximately 1 cm panel dimension for each meter of elevation from the ground.

Results from Fig. 2.3 and Fig. 2.4 tell us that care must be taken when analyzing results for small ( $<1$  m) panels. We assume binary direct shadowing in this model. In experiments, we expect shadow edge softening that can be confirmed by observation and a corresponding gradient of irradiance that is not reflected by the harsh lines caused by this binary direct shadowing assumption.

### 2.1.4 Electrical Power Model

Power capacity as a function of time,  $P_{PV}(t)$ , is calculated using a light intensity dependent solar cell model [23] to account for the varying light intensity over the course of a day and to compare power capacity across locations.

The concentration factor  $X$  is calculated using time-dependent GHI ( $\text{W}/\text{m}^2$ ) with a reference of 1 sun ( $1000 \text{ W}/\text{m}^2$ ):

$$X(t) = \frac{GHI(t)}{1000} \quad (2.16)$$

Open circuit voltage ( $V_{OC}$ ) short circuit current ( $J_{SC}$ ), and fill factor are then adjusted accordingly, assuming an ideality factor  $n = 1$  and a temperature of 300 K:

$$V'_{OC}(t) = V_{OC} + \frac{nkT}{q} \ln(X(t)) \quad (2.17)$$

$$J'_{SC}(t) = J_{SC}X(t) \quad (2.18)$$

$$v'_{OC}(t) = \frac{q}{nkt} V'_{OC} \quad (2.19)$$

$$FF'(t) = \frac{v'_{oc}(t) - \ln(v'_{oc}(t) + 0.72)}{v'_{oc}(t) + 1} \quad (2.20)$$

$$\eta'(t) = \frac{V'_{OC}(t)J'_{SC}(t)FF'(t)}{GHI(t)} \quad (2.21)$$

Power calculations are then performed based on the angle of incidence (AOI) between solar rays and the panel for tracking and fixed-tilt modes. AOI is determined using PVLlib [36]. Power is calculated in terms of W per  $\text{m}^2$  of land because agri-voltaics are land area dependent systems [3]. As such, the ground coverage ratio, also known as packing fraction, is calculated and defined as the ratio between PV area,

$A_{PV}$  and ground area. For the infinite periodicity mode with unit cell of dimensions  $p_{NS}$  and  $p_{EW}$ , this is:

$$GCR = \frac{A_{PV}}{(p_{NS})(p_{EW})} \quad (2.22)$$

Note that this formulation assumed that all PV area contributes to power capacity.

$$P_{dir}(t)[W/m^2 \text{ of land}] = \eta'(t)DNI(t) \cos(AOI)(GCR) \quad (2.23)$$

The Perez model is used to determine the fraction of diffuse light incident on the panel surface. Blocking of light from other PV panels is not accounted for.

$$P_{dif}(t)[W/m^2 \text{ of land}] = \eta'(t)DHI_{PV,Perez}(t)(GCR) \quad (2.24)$$

Daily power capacity is the sum of  $P_{dir}(t)$  and  $P_{dif}(t)$  averaged over 24 hr. Table 2.1 lists the IV characteristics used for power capacity calculations in this work, indicative of high efficiency commercial silicon PV modules [42].

Table 2.1.: Device IV Characteristics for Electrical Power Model

Parameter	Value
$V_{OC}$	0.7 mV
$J_{SC}$	40 mA/cm <sup>2</sup>
FF	80 %

### 2.1.5 Code Availability and nanoHUB Tool

An online accessible closed source tool to use this program is available online at [nanohub.org/tools/agpvsim](https://nanohub.org/tools/agpvsim) with a corresponding user guide. Code is available in a Git repository upon request.

## 2.2 Estimating Crop Yield

As described in Chapter 1, shading conditions can have significantly varied effects on crops. In many cases, a given shading condition can have both negative and positive effects [10]. Both the temporal variation of shading and the shading intensity affect crop growth, however the literature is not sufficiently comprehensive or conclusive to use simple metrics to accurately estimate crop yield. Complex crop models are typically used to predict performance for various microclimate conditions, include radiation levels [7, 10].

The purpose of this work is to analyze irradiance distributions in APV systems at both the crop and PV level. Utilization of crop models for specific case studies or generalized modeling is beyond the scope of this thesis. In lieu of more accurate yield predictions, estimates of yield can be inferred using photosynthetic rate vs. levels of photosynthetically active radiation with subsequent saturation irradiance levels. To this end, we calculate the fractional reduction in insolation integrated for a single day (called ‘shadow depth’) and assume yield is proportional to this metric.

### 3. DESIGNING OPTIMIZED AGRIVOLTAIC STRUCTURES FOR COPRODUCTION OF SOLAR ENERGY AND CROP BIOMASS

In this section, field irradiance distributions and the trade-offs between APV power production and expected crop yield are analyzed. We first investigate the effects that PV array configuration has on underlying field irradiance. Array-level parameters of row spacing, panel width, and panel orientation are investigated and compared to experimental data in the literature. We then explore how novel geometric panel patterns that utilize ‘mini modules’ affect field irradiance metrics. Promising patterns and configurations are then explored in detail.

#### 3.1 Effects of PV System Configuration

System configuration perhaps plays the most influential role in determining the radiation spatial distribution in the agricultural field. Existing experimental agrivoltaic systems that use fixed tilt south-facing panels have measured significant periodic non-uniformity in radiation along the N-S axis [14, 15]. We corroborate this periodic spatial non-uniformity in radiation via simulation (Fig. 3.1), showing that high levels of spatial non-uniformity in integrated radiation, in  $\text{J}\cdot\text{m}^{-2}\text{d}^{-1}$ , occur in the presence of PV arrays.

An elevated fixed latitude-tilt south-facing array with high row width was modeled for three major agricultural regions in the U.S.: West Lafayette, IN (40.4, -86.6); Fresno, CA (36.6, -119.9); and Lubbock, TX (33.5, -101.8). Fig. 3.1(Case A) shows a spatial map of the resulting shadow depth on June 1, 2018 for the Texas region. We see that this configuration (1.5 m panel width, 5 m height, 7.62 m row width) produces regions of high shadow depth, dubbed shadow trenches, which can reach upwards of

60% when integrated over a single day. Elevated E-W tracking configurations were explored (Fig. 3.1(Case D, Case E)) showing similar net losses in radiation, however insolation homogeneity, given by the spatial standard deviation in shadow depth, and PV power production increased (Table 3.2). High insolation homogeneity is expected due to the east-west nature of diurnal shadow migration, and may explain the decreased yield of agrivoltaic systems that implemented south-facing structures [4]. Marrou (2013) detected, in experimental south-facing agrivoltaic systems, high periodic spatial variability and a decrease of nearly half of available sunlight for high-density ( $GCR = 0.5$ ) systems. Valle (2017) measured homogeneous insolation for their E-W tracking APV systems [15], corroborating the results of this model.

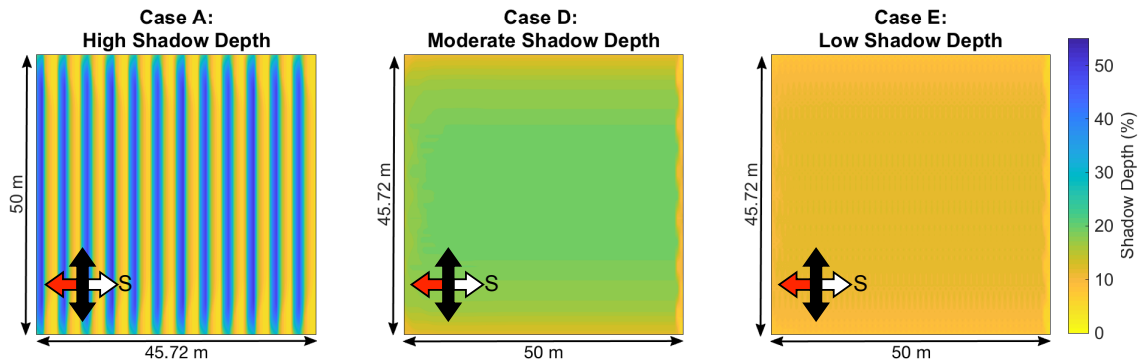


Fig. 3.1.: Shadow depth of different configurations in West Lafayette, IN. [30]. PV system parameters in Table 3.1. Case E utilizes checkerboard patterning elaborated on in section 3.3.

The model implemented assumes that diffuse irradiance reaches the ground uniformly due to the exceptional height of simulated systems (5 m). Based on this assumption, days and regions with low values of diffuse index,  $k_d$ , will show higher spatial and temporal non-uniformity in radiation. This is demonstrated in Table 3.2 for regions with high  $k_d$  (Indiana), moderate  $k_d$  (Texas), and low  $k_d$  (California). In Table 3.2, fixed south-facing configuration is at a latitude-tilt, and E-W tracking configuration has  $90^\circ$  tracking range. Higher  $k_d$  corresponds with higher standard de-

Table 3.1.: Parameters and metrics for systems in Fig. 3.1 and related [3].

	Configuration	Panel pattern	Row spacing (m)	Average shadow depth (%)	Shadow depth s.d.(%)	Land with less than 25% shadow depth (%)
A	South facing	None	3.81	35.2	15.2	41.0
B	South facing	Checker	3.81	17.6	7.6	74.7
C	EW tracking	None	3.81	31.5	0.6	0
D	EW tracking	None	7.62	21.4	0.6	100.0
E	EW tracking	Checker	7.62	11.5	1.1	100.0

viation (i.e. less spatial homogeneity) for fixed-tilt south-facing systems. However, higher  $k_d$  also corresponds with lower average insolation loss.

Table 3.2.: PV effects on insolation for different locations and diffuse indices.

Configuration	Location	$k_d$ [32]	Shadow Depth mean	Shadow Depth s.d.	Power (W/m <sup>2</sup> )
Fixed S-facing	CA	0.19	34.6%	20.8%	16.6, 22% from DNI
E-W tracking	CA	0.19	27.2 %	0.8%	22.2, 20% from DHI
Fixed S-facing	TX	0.31	35.2%	15.2%	11.8, 45% from DHI
E-W tracking	TX	0.31	31.5%	0.6%	15.1, 41% from DHI
Fixed S-facing	IN	0.41	35.0%	10.1%	8.1, 62% from DHI
E-W tracking	IN	0.41	34.6%	0.3%	10, 43% from DHI

### 3.1.1 Case study: ACRE Farm

In this section, spatial maps of the modeled cumulative radiation spatial distribution in an experimental agrivoltaic system at Purdue University are presented,

demonstrating the impact of edge effects on the irradiance distribution and other spatial metrics in agrivoltaic systems. This is of utmost importance to understand because most agrivoltaic research plots are small-scale (Table 1.2), creating significant edge effects across the growing season that must be accounted for.

The ACRE system utilizes parameters (Table 3.3) that are believed to be conducive to the needs of crops that require high levels of irradiance, such as maize, and implements novel panel geometric arrangements proposed in [3]. Half of each PV row, referred to as pattern A, utilizes conventional full size 72-cell modules. The other half, pattern B, utilizes a checkerboard pattern with half size 36-cell modules. The panel outlines at 0° tilt are overlaid on the radiation spatial maps in Fig. 3.2. Only direct radiation and the corresponding shadow depth from direct radiation is considered in this study. Diffuse light is expected to remain relatively homogeneous for these plots, but only due to this system’s low GCR (0.165 and 0.076, respectively for patterns A and B) and high (6 m) height from the ground, as per analytical analysis of diffuse light in APV systems in [6].

Table 3.3.: Purdue ACRE Agrivoltaic System Parameters.

Parameter	Value
Height	6 m
PV row spacing	9.91 m
PV row length	14.5 m
PV width (A, B)	1.778 m, 1.5 m

It is visually evident that, even with 4 rows of PV panels, edge effects play a major role in the radiation distribution for pattern A both temporally and spatially. For pattern B, the difference is less extreme due to the lower ground coverage ratio. This case study emphasizes the importance of modeling irradiance distributions for the entire growing seasons in small-scale agrivoltaic systems.

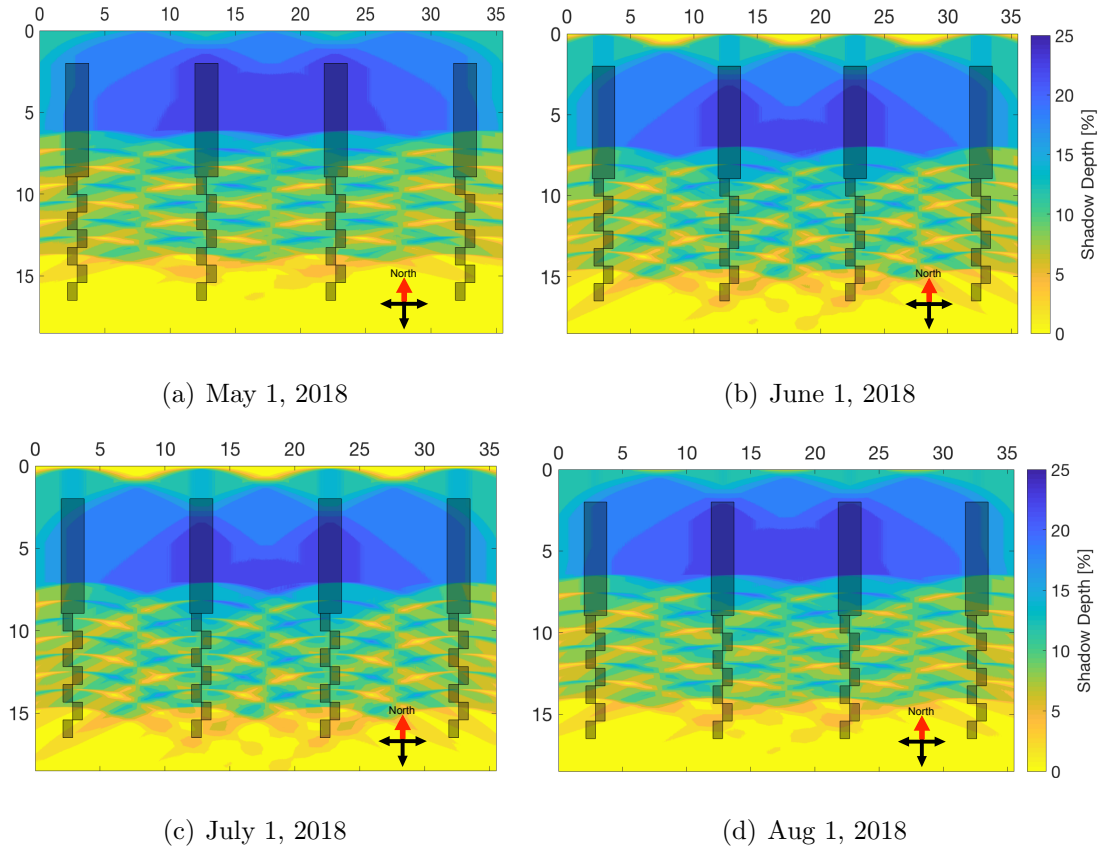


Fig. 3.2.: Direct shadow depth spatial maps at Purdue ACRE farm for four months of the growing season: a) May 1, 2019, b) June 1, 2018, c) July 1, 2018, and d) August 1, 2018. Photovoltaic panels are displayed in semi-transparent gray at  $0^\circ$  tilt from the horizontal.

### 3.2 Row Width, Panel Width

To better understand how array configuration affects field insolation and output power, the parameters row width and panel width were examined. From the shadow depth spatial distribution map of a south-facing system (Fig. 3.1(a)), it is evident that increased panel width will widen the high-loss 'shadow trench' and that increased PV row spacing will separate the 'shadow trench' rows. To quantify their effects, the metrics shadow depth and shadow duration vs. power density (capacity) are used.

It is known and intuitive that increasing the distance between panel rows, also known as row width, increases the radiation available per unit area to crops [6, 7, 13, 15]. Here we calculate a  $\frac{1}{r}$  dependence of shadow depth on row spacing. The reason is that, by law of energy conservation and the model assumption of complete absorption described in Chapter 2, shadow depth is directly proportional to the GCR, which is inversely proportional to row width (Eqn. 2.22). Note that the exact relationship between shadow depth and row width requires modifications for solar angle of incidence on the panel, and for direct and diffuse radiation as functions of time and space in the solar dome.

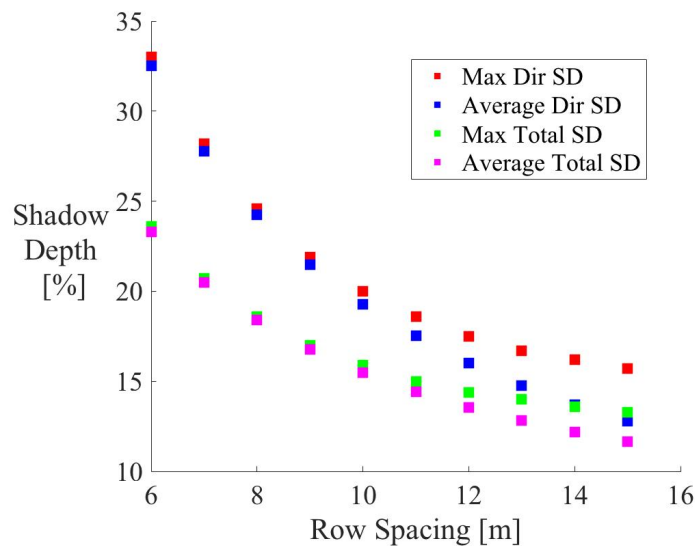


Fig. 3.3.: Effect of row width on shadow depth.

Fig. 3.3 shows row width vs. shadow depth for an E-W tracking system on June 1, 2018 in West Lafayette, IN. E-W tracking was chosen because of the high spatial uniformity. However, this spatial uniformity breaks down at high row spacing due to the temporally-changing relationship between shadow position and irradiance levels over a given day. This is because shadow depth is a function of cumulative time in shadow and irradiance as a function of time (Eqn. 2.12, Eqn. 2.15).

By increasing panel width, agrivoltaic systems can generate more electricity by the principle that PV area is directly proportional to power generation due to the increased area of PV intercepting radiation. However, the cost is decreased total radiation available to crops and increased duration of shadowing over a given region of the field. In Fig. 3.4, a very large row spacing of 10 m was used to isolate shadowing effects of adjacent PV rows. Infinite PV axis length was used to ensure variation along a single cardinal axis for each system, mimicking a 2D simulation.

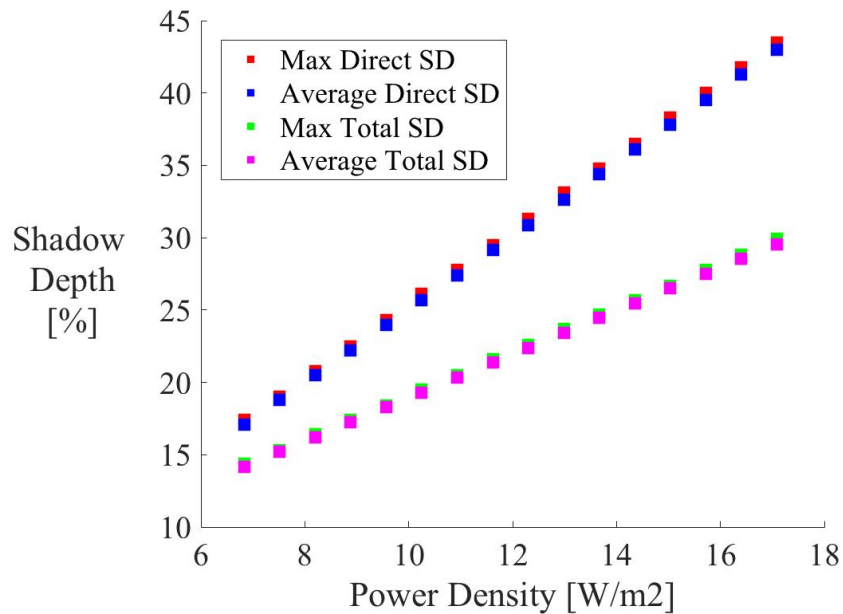


Fig. 3.4.: Effect of panel width on shadow depth.

The ratio of panel width to row spacing can give insight into trends of radiation distribution and shadow duration. Fig. 3.4 shows the east-west tracking system with varying panel width and row width to demonstrate the variation in spatially averaged shadow depth, temporal variation in shadow depth, and shadow duration over given points in the field. Infinitely periodic rows of PV were simulated to demonstrate effects of a realistic PV farm.

### 3.3 Panel Patterning

In this section, different panel patterns (Fig. 3.5) are explored for a given set of array-level parameters. Since it was found in the previous section that E-W systems outperform fixed-tilt south-facing systems in terms of insolation homogeneity, results in this section emphasize E-W tracking systems. Tracking parameters are listed in Table 3.4.

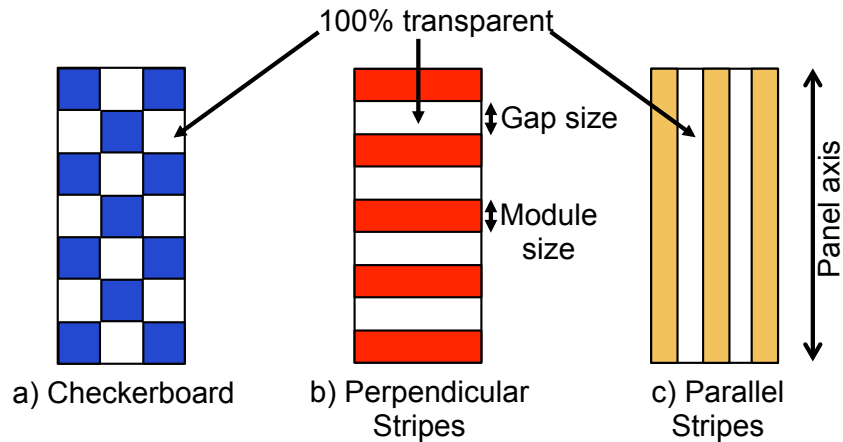


Fig. 3.5.: Panel patterns.

Table 3.4.: Tracking Parameters for data set in Fig. 3.6, Fig. 3.7, Fig. 3.8, and Fig. 3.9.

Parameter	Value
Rotation Axis	Single, N-S axis
Backtracking	Off
Max Angle	45°
Panel Width	Varied
Panel Length	Infinite

To understand the operating regimes for different panel patterns in the E-W tracking configuration, multiple panel dimensions and corresponding ground coverage ratios were explored. Optimizing the trade-off between power spatial density and shadowing effects is a multi-objective problem with no inherent constraints, therefore Pareto front optimization is used in this analysis. In this method, a data point,  $a$ , is considered dominant over another data point,  $b$  if it is closer to the origin in both axes. A data point,  $a$ , that is closer in one axis to another data point,  $c$ , but is further in the other axis, may be considered along the Pareto front, given that no other data points are dominant over it.

It is found that average shadow depth has a linear relationship with power density (Fig. 3.6). This is expected because, with all tracking and electrical parameters remaining fixed across systems, the law of energy conservation defines a linear relationship between irradiance incident on the panels and irradiance incident on the field. When this irradiance is integrated and averaged, a linear relationship between average shadow depth and power density is observed. Of interest is the dependence of slope on location for a given day of year. The diffuse fraction,  $k_d$ , and the total GHI dictates this relationship. Regions with low GHI, such as in Indiana, have lower power density. Fig. 3.6(a-c) shows this trade-off for June 1, 2018, where smaller  $k_d$  has a larger slope. Fig. 3.6(d-f) shows that shadow depth remains approximately constant across systems and locations with only power differing, and analysis indicates the difference is due to small variations in solar migration paths. This data supports the claim that APV systems regions with high GHI and high  $k_d$  may have the highest performance.

Panel pattern is shown to have a significant and consistent effect on shadow depth spatial homogeneity. Spatial homogeneity is given by the spatial standard deviation in shadow depth plotted in Fig. 3.7. It is evident that the parallel stripes pattern produces the most homogeneous shadowing, below 3% in TX, CA, and IN locations when including contributions from diffuse light (Fig. 3.7(a-c)), and below 4% when only considering direct light contributions (Fig. 3.7(d-f)).

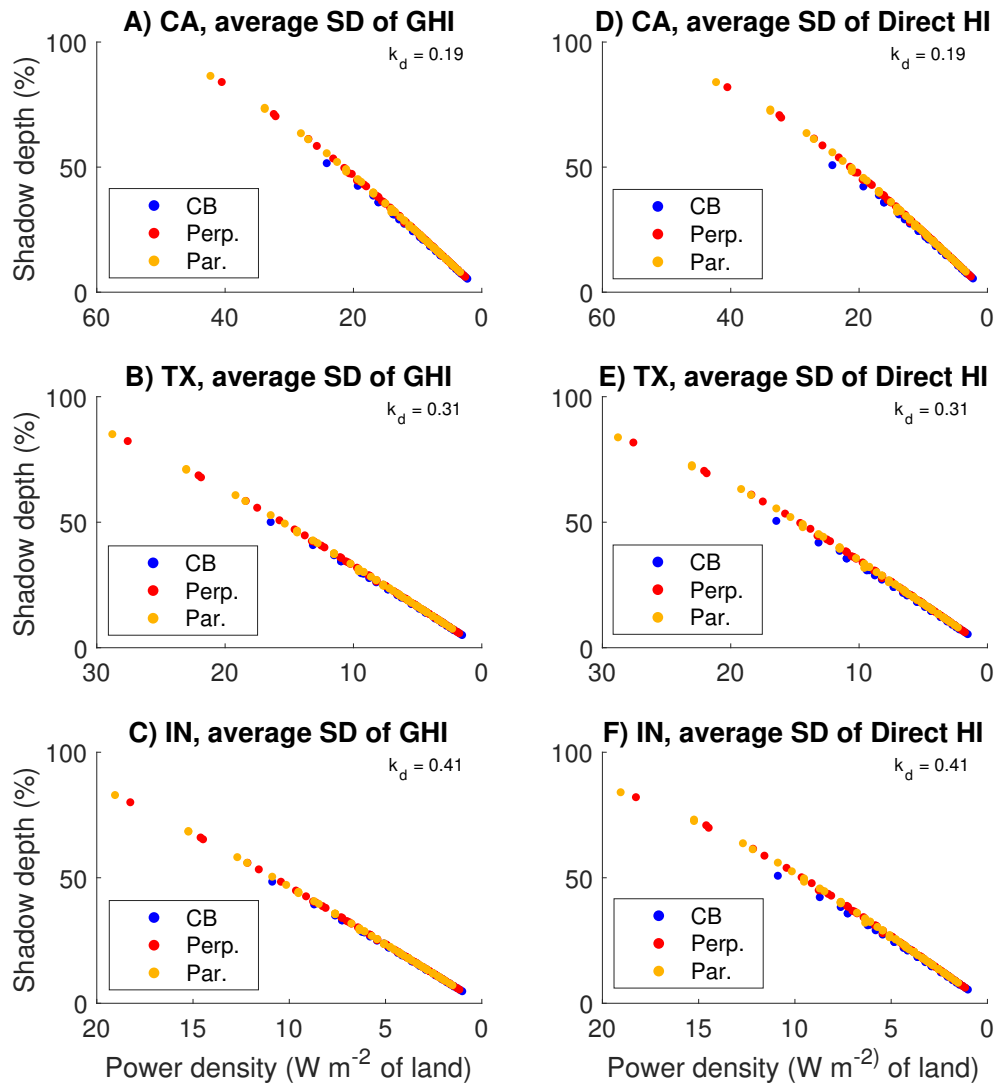


Fig. 3.6.: Pareto front visualization of shadow depth average vs. spatial power density, simulated for June 1, 2018. Shadow depth from GHI given in (a-c); shadow depth from direct horizontal irradiance only given in (d-f) for California ( $k_d=0.19$ ), Texas ( $k_d=0.31$ ), and Indiana ( $k_d=0.41$ ) locations. Checkerboard (CB), perpendicular (perp.) and parallel (par.) patterns shown.

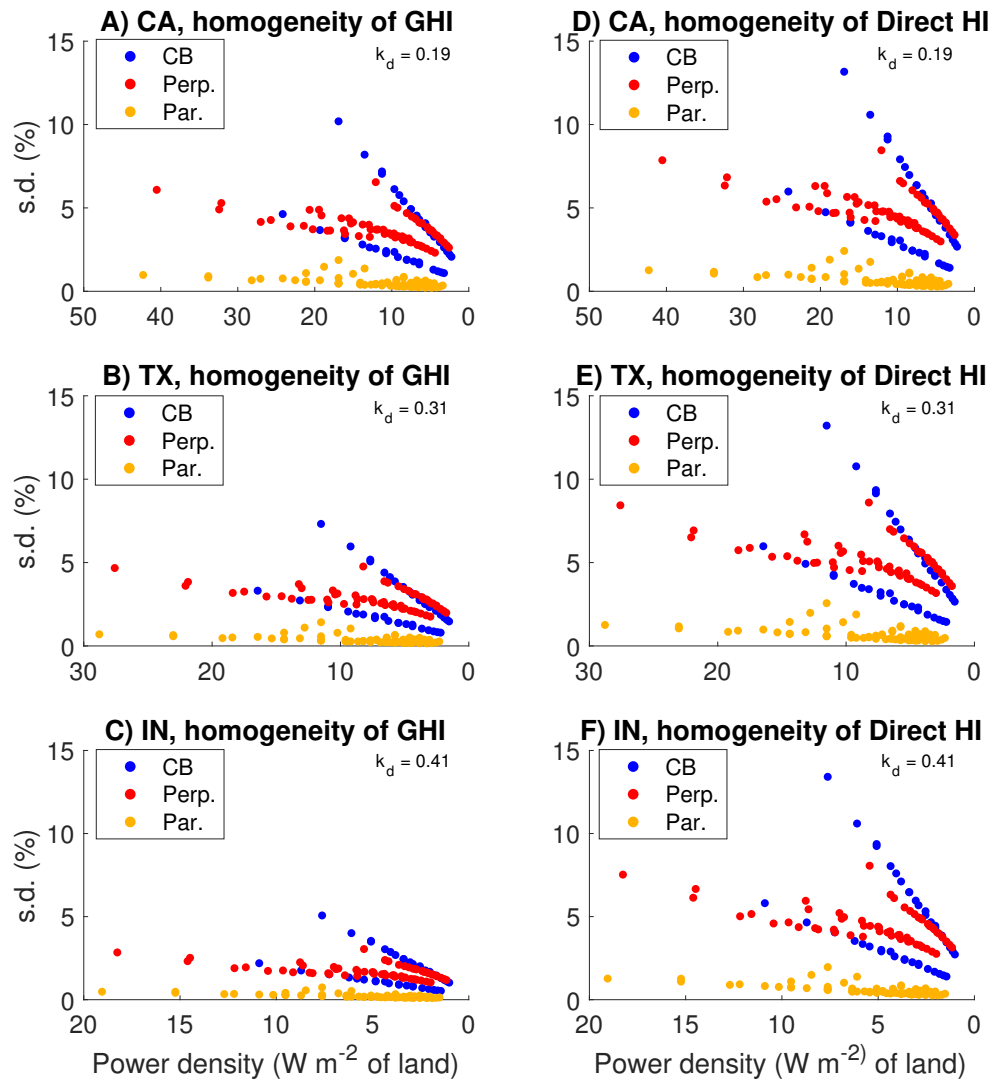


Fig. 3.7.: Pareto front visualization of shadow depth homogeneity (spatial standard deviation) vs. spatial power density, simulated for June 1, 2018. Shadow depth from GHI given in (a-c); shadow depth from direct horizontal irradiance only given in (d-f) for California ( $k_d=0.19$ ), Texas ( $k_d=0.31$ ), and Indiana ( $k_d=0.41$ ) locations. Checkerboard (CB), perpendicular (perp.) and parallel (par.) patterns shown.

For the temporal component of APV shadowing, Fig. 3.8 shows shadowing from sunrise to sunset and Fig. 3.9 shows shadowing during peak irradiance hours, 10 a.m.

to 4 p.m. local time. The average maximum shadow duration at each point in the plot is less for midday shadows than full-day shadows for all cases. This is because mutual shading of PV panels couples otherwise distinct shadows. For parallel stripes, this effect is enhanced in the spatial standard deviation of maximum shadow duration in the plot (Fig. 3.9(d-f)). Upon analysis, we see mutual shading is eliminated for most cases, leaving panel width as the primary influencing factor for shadow duration.

Table 3.5.: Input parameters for parallel and perpendicular stripes data sets in Fig. 3.7, Fig. 3.6, Fig. 3.8, and Fig. 3.9. The same panel dimensions are used for both systems. Length is varied to ensure proper infinite periodicity of each pattern, not affecting results that are per unit area.

Panel width	Module size	Gap size	no. stripes	Row spacing (m)
1.90 m	0.50 m	0.20 m	3	4, 5, 6, 7, 8, 9, 10
1.30 m	0.30 m	0.20 m	3	4, 5, 6, 7, 8, 9, 10
2.30 m	0.30 m	0.20 m	5	4, 5, 6, 7, 8, 9, 10
1.60 m	0.40 m	0.20 m	3	4, 5, 6, 7, 8, 9, 10
3.00 m	0.20 m	0.50 m	5	4, 5, 6, 7, 8, 9, 10
2.60 m	0.20 m	0.50 m	4	4, 5, 6, 7, 8, 9, 10
1.90 m	0.20 m	0.50 m	3	4, 5, 6, 7, 8, 9, 10
3.45 m	0.75 m	0.15 m	4	4, 5, 6, 7, 8, 9, 10
2.85 m	0.60 m	0.15 m	4	4, 5, 6, 7, 8, 9, 10

### 3.3.1 Checkerboard Pattern

Examining the effects of checkerboard pattern in isolation, we look at the blue data sets in Fig. 3.7. Two designs with checkerboard pattern of dimension 0.25 m by 0.25 m and 0.5 m by 0.5 m checkers are shown. Higher dimension checkerboard

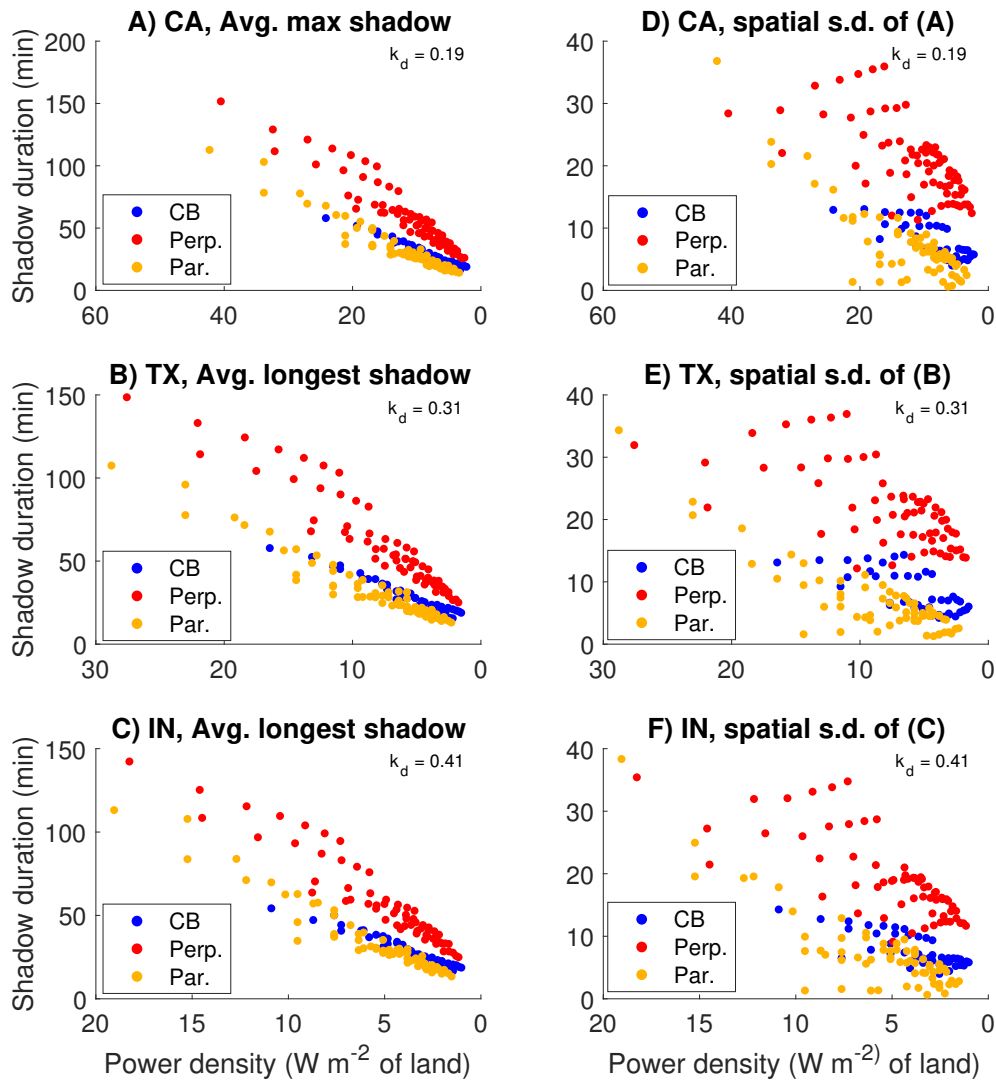


Fig. 3.8.: Pareto front visualization of spatially averaged maximal shadow duration for each field finite element from sunrise to sunset vs. spatial power density, simulated for June 1, 2018. Standard deviation of this spatial average shown in (D-F). Minimal shadow duration and maximal power production are desired for optimal APV system performance. Checkerboard (CB), perpendicular (perp.) and parallel (par.) patterns shown.

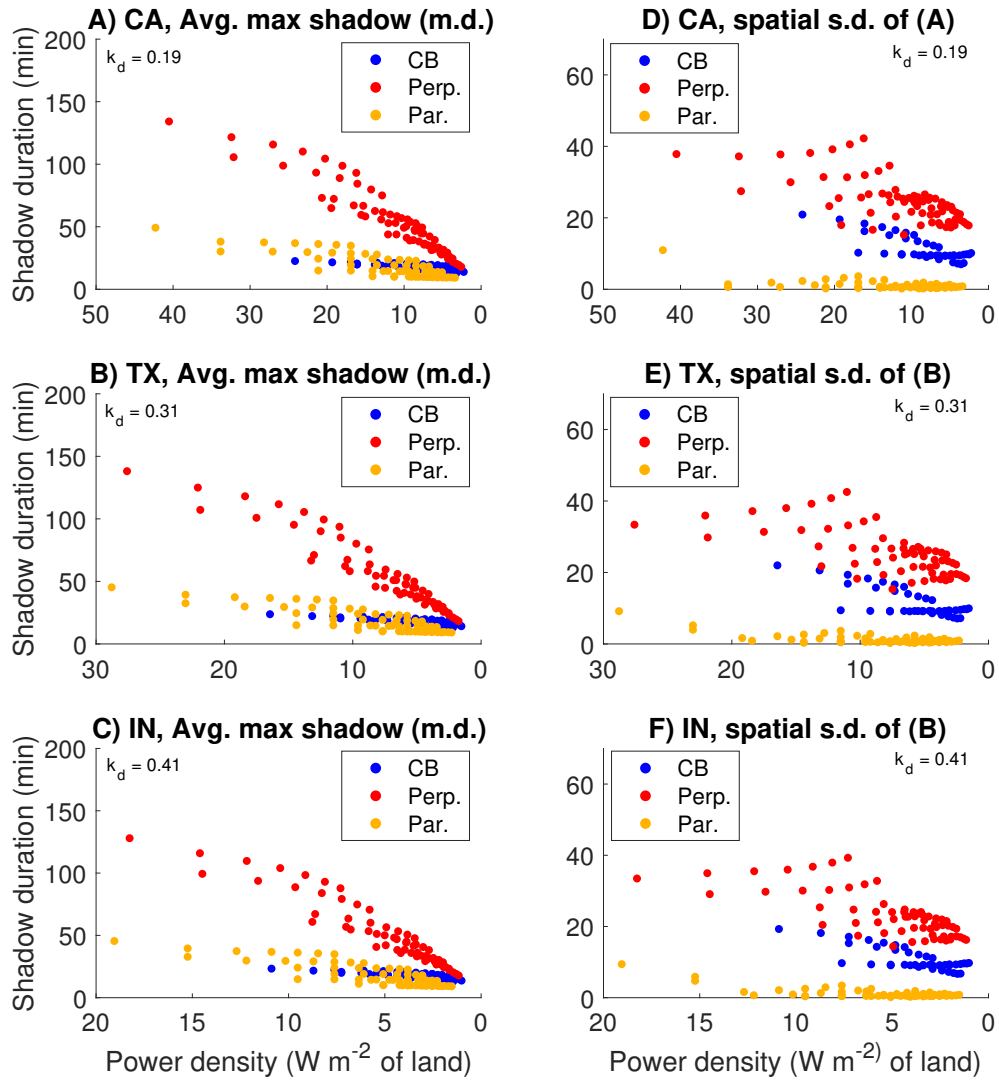


Fig. 3.9.: Pareto front visualization of spatially averaged maximal shadow duration for each field finite element from 10 a.m. to 4 p.m. local time vs. spatial power density, simulated for June 1, 2018. Standard deviation of this spatial average shown in (D-F). Minimal shadow duration and maximal power production are desired for optimal APV system performance. Checkerboard (CB), perpendicular (perp.) and parallel (par.) patterns shown.

pattern (0.5 m by 0.5 m) has a higher slope proportional to the row spacing (lower row spacing has higher spatial power density for the same panel system). By reducing the checker dimension by a factor of 2, and subsequently the area of each PV checker by a factor of 4, shadow depth standard deviation is decreased by more than half.

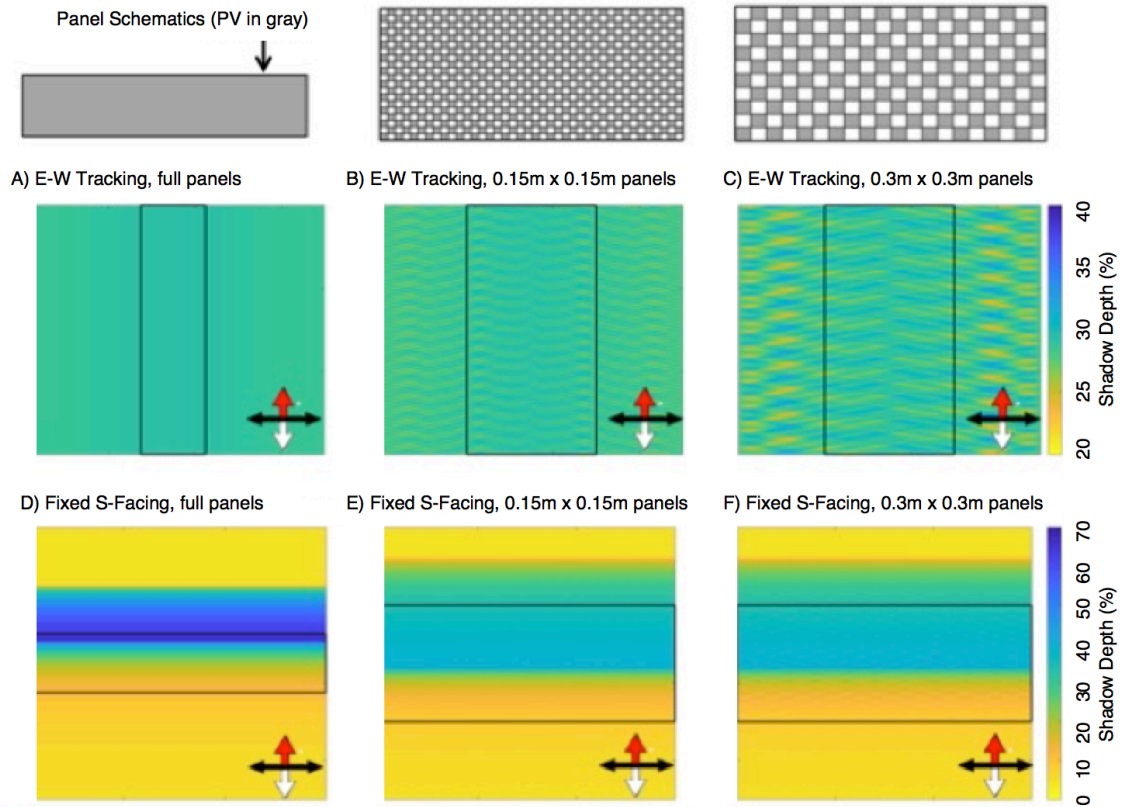


Fig. 3.10.: Effect of checkerboard dimensions on shadow depth [30].

We explored the effects of the checkerboard design further in east-west tracking systems by varying the mini-module dimensions (Fig. 3.11). This metric allows us to observe the “worst case” spatially for a given agrivoltaic system. We demonstrate that, while power production will correspondingly vary, shadow depth can be manipulated by varying the photovoltaic module dimensions. It is also demonstrated that regions with smaller fractions of diffuse light (Fresno, CA) are more impacted by agrivoltaic system shadowing effects. For long rectangular checkerboards with the

same PV area, we see that increasing the N-S dimension from 1 to 5 m increases the maximum shadow depth by an absolute 10%. Panel width is fixed at 1.5 m and row spacing is fixed at 7.62 m.

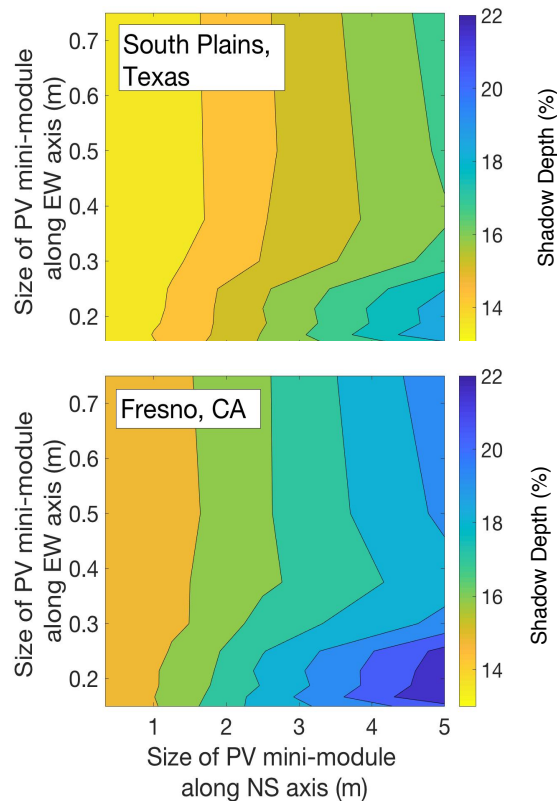


Fig. 3.11.: Effect of checkerboard dimensions on shadow depth [30].

Examining the effects of checkerboard on shadow duration, we find that smaller checkerboard dimensions create shorter average maximum shadow duration. Fig. 3.12 shows binary time-series data for representative points in the field where black indicates that the point is in direct shadow. For the fixed-tilt south-facing system, the representative point is within the shadow trench where the majority of shadowing occurs. It is shown that fine checkerboard pattern decreases average shadow duration by multiple hours. For the E-W tracking system, average maximum shadow duration does decrease, but the temporal distribution varies. The spatial homogeneity in E-W tracking systems is distributed over the entire plot rather than a sub-area, the

‘shadow trench’, in fixed-tilt south-facing systems because the PV length extends over the entire N-S axis. Therefore, the temporal variation in shadow depth is dependent on the spatial position examined for E-W tracking systems.

We conclude that checkerboard pattern decreases average shadow duration and improves shadow homogeneity (Table 3.6). Though total radiation incident on the field will be maintained for a given PV area and array configuration, the temporal distribution can be controlled by using this checkerboard pattern. It should be noted that in practice, direct shadow duration will be shorter due to the plane source approximation error explained in Chapter 2.

Table 3.6.: Checkerboard Shadow Effects. Spatial average and standard deviation in shadow depth. Spatially average maximum shadow duration in time for midday and full day [30].

<b>Texas</b>	<b>Shadow Depth (%)</b>	<b>Midday (10AM- 4PM) (min)</b>	<b>Full Day (min)</b>
E-W tracking, full panels	$28.9 \pm 0.4$	$69.7 \pm 2.6$	$71.3 \pm 1.5$
E-W tracking, 0.15m x 0.15m	$28.6 \pm 1.0$	$9.8 \pm 2.9$	$40.6 \pm 9.1$
E-W tracking, 0.3m x 0.3m	$28.6 \pm 1.5$	$15.8 \pm 3.7$	$38.6 \pm 8.6$
Fixed S-facing, full panels	$18.8 \pm 19.3$	$67.1 \pm 126.4$	$98.1 \pm 128.4$
Fixed S-facing, 0.15m x 0.15m	$18.8 \pm 13.1$	$4.4 \pm 4.8$	$16.6 \pm 3.1$
Fixed S-facing, 0.3m x 0.3m	$18.8 \pm 13.1$	$7.4 \pm 8.0$	$17.1 \pm 3.1$

### 3.3.2 Parallel Stripes

It is shown in Fig. 3.13 that parallel N-S axis stripes in N-S axis tracking systems have the most uniform shadow depth. However, this shadowing effect has an optimal

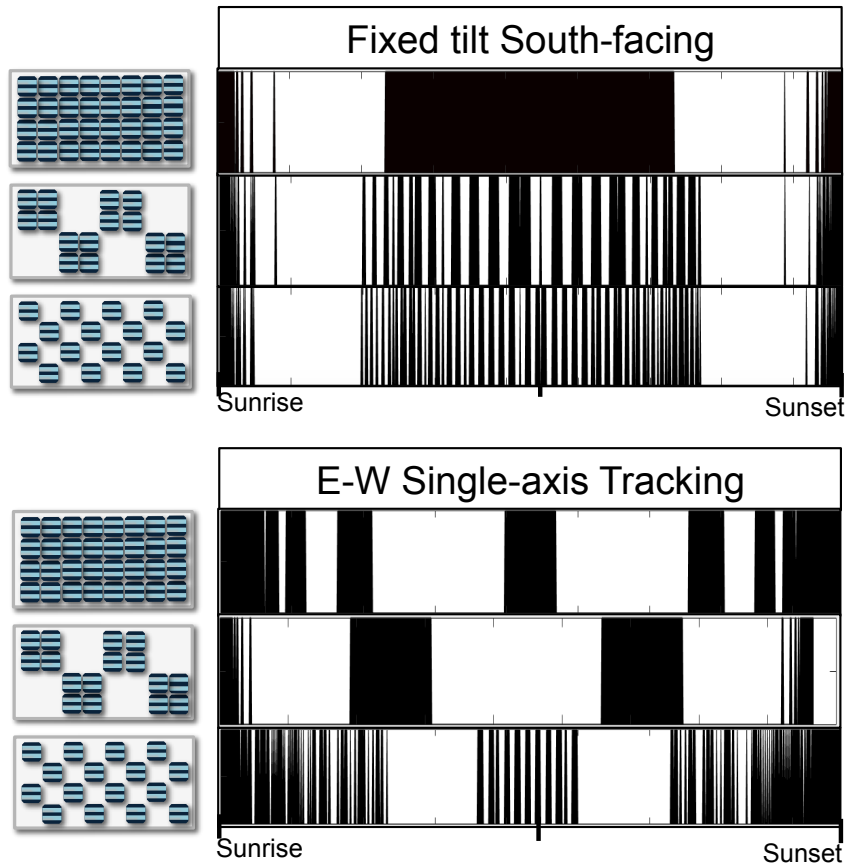


Fig. 3.12.: Effect of checkerboard dimensions on shadow duration [30]. Time-series data for the California location on June 1, 2018. Black indicates direct shadow. Checkerboard dimensions are 0.15m x 0.15m and 0.3m x 0.3m and the same PV area is used (1.5m width vs. 3m width for 50% PV density checkerboard).

row width. Fig. 3.13 shows varied homogeneity for different row widths where each color indicates a different pattern. Though there is an optimal value for highest homogeneity, the difference is so small (1.5%) that we anticipate no significant variation in experiment.

The parallel stripes pattern in the E-W tracking configuration is shown to provide the highest field insolation spatial homogeneity. This pattern also offers direct control of shadow duration.

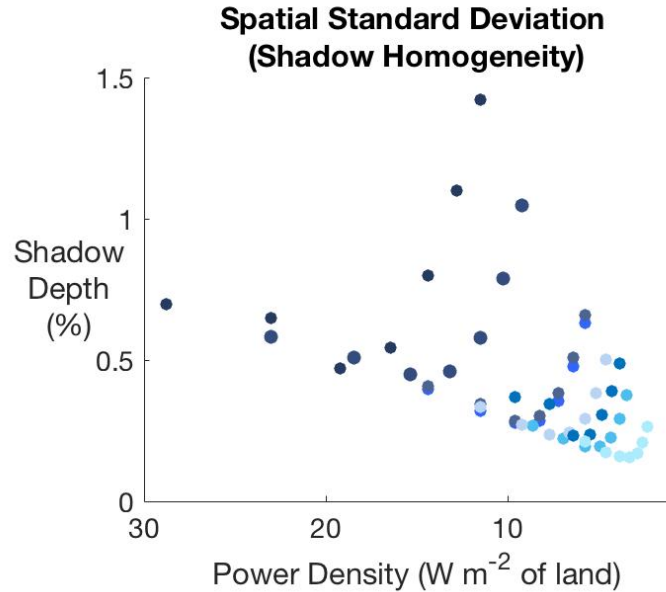


Fig. 3.13.: Homogeneity of parallel stripes vs. row width. Each color is a different data set from Table 3.5. The minima correspond to the 7 m row width for the Indiana location on June 1, 2018.

### 3.4 Summary and conclusions

In this chapter, a range of APV array configurations, with varying panel width, row spacing, and panel patterns were simulated to predict their effect on field irradiance distributions and spatial power density. Based on this study, it is clear that south-facing configurations produce regions of high shadow depth. East-west tracking configurations provide increased spatial power density from the added tracking, and create highly homogeneous radiation distributions on the field. Panel patterning shows that while overall shadow depth is maintained for a given PV area and configuration, patterning can affect radiation homogeneity and shadow duration. Temporal data shows that spacing the PV modules along the E-W PV axis reduces shadow duration over a given point in the field, barring elongation from shadow overlap in PV mutual shading conditions.

It is recommended that APV design incorporate panel patterning when shadow duration is of concern. Parallel stripes and checkerboard pattern may be most physically realizable from a circuitry perspective. It is also recommended that APV systems be installed facing east-west (rather than south) if shadow homogeneity is required.

## 4. TRACKING ALGORITHMS TO MANIPULATE SHADOWS

Solar tracking algorithms can be implemented to manipulate the amount and duration of intercepted radiation by the PV array to optimize plant growth. Valle (2017) demonstrated this experimentally by using a controlled tracking system with the intentions of minimizing morning and evening shading and maximizing midday shading to reduce adverse affects of high irradiance [15]. Controlled tracking (CT) in a 3-row dynamic APV system was implemented by moving the photovoltaic panels nearly parallel to incoming solar rays ( $90^\circ$  away from conventional solar tracking) in the morning and evening, with conventional solar tracking implemented from 11 a.m. to 4 p.m. [15]. To compare, they implemented a standard solar tracking (ST) 4-row PV array and a fixed-tilt high density (HD) PV array (1.6 m row spacing). They measured +51% and +18% increases in electricity for ST and CT, respectively, on a cloudy day relative to HD electricity production and +74% and -23% electricity production, respectively, for a sunny day. For field irradiance, CT transmitted approximately 80% of total radiation in spring and summer while ST transmitted approximately 60%. Transmitted radiation was converted into biomass (biomass (g)/cumulative radiation (mol)), showing a statistically significant difference between CT, and ST, with CT exhibiting results statistically similar to the full sun control group.

From these results, it is evident that APV systems with controlled tracking algorithms that minimize radiation loss on the field have the potential to effectively mirror agricultural production in full sun conditions while generating electricity. Furthermore, these algorithms may be most useful in cloudy conditions with bifacial panels to maximize electricity output [15].

## 4.1 AOI Manipulation

Maximizing the angle of incidence, AOI, up to  $90^\circ$ , between the solar ray and the photovoltaic, PV, module active face normal at a given time minimizes direct shadow area on the field created by an elevated PV module and minimizes intercepted radiation. Subsequently, maximizing this angle of incidence minimizes the direct radiation loss on the field due to PV module radiation interception. Radiation energy  $E_{tot}$  available to the field is defined as:

$$E_{tot} = \int_{t_1}^{t_2} I_{GHI}(t) A_{field} dt, \quad (4.1)$$

where  $A_{field}$  = total area of the field.

The intercepted radiation by the PV module over a time period from  $t_1$  to  $t_2$  is given by the equations:

$$E_{PV,direct} = \int_{t_1}^{t_2} I_{DNI} A_{PV} \sin AOI(t) \alpha(AOI) dt \quad (4.2)$$

$$E_{PV,diffuse} = \int_{t_1}^{t_2} I_{DHI} A_{PV} f(AOI(t)) \alpha(AOI) dt \quad (4.3)$$

$$E_{PV} = E_{PV,direct} + E_{PV,diffuse} \quad (4.4)$$

where:

$E_{PV}$  = Energy intercepted by the PV module

$E_{PV,direct}$  = Energy intercepted by the PV module from direct solar rays

$E_{PV,diffuse}$  = Energy intercepted by the PV module from diffuse solar rays

$A_{PV}$  = Area of a PV module face

$\alpha$  = Angular-dependent absorption coefficient of PV module

$f$  = Fraction of diffuse irradiance intercepted by the PV module, dependent on AOI

Radiation available to the field is then given by:

$$E_{field} = E_{tot} - E_{PV} - E_{r,atmosphere} \quad (4.5)$$

where  $E_{r,atmosphere}$  is energy from solar radiation reflected back to the atmosphere.

According to the Perez model, diffuse light is maximal around the solar disc, decreasing with distance away from the solar disc in the celestial sphere [39]. We can then assume that the factor  $f(AOI)$  will mimic the behavior of the angular term,  $\sin AOI$  in Eqn. 4.2. Therefore, barring abnormalities from weather patterns, maximization of the AOI of direct solar rays on the PV module active face to minimize shadow area will also minimize diffuse radiation loss on the field due to PV module radiation interception. The active face is the width by length face (both sides in a bifacial PV module, one side in a monofacial PV module, which is primarily responsible for generating the majority if not all of the electricity), and the inactive faces are the width by thickness and the length by thickness faces. AOI (Fig. 4.1, Fig. 4.2) is defined in [44] as:

$$AOI = \arccos [\cos T_m \cos Z_s + \sin T_m \sin Z_s \cos (AZ_s - AZ_m)] \quad (4.6)$$

where:  $AOI$  = Solar angle of incidence on PV module (deg)

$T_m$  = Tilt angle of module ((deg),  $0^\circ$  is horizontal)

$Z_s$  = Solar zenith angle (deg)

$AZ_s$  = Solar azimuth angle ((deg), North= $0^\circ$ , East= $90^\circ$ )

$AZ_m$  = PV face azimuth angle ((deg), North= $0^\circ$ , East= $90^\circ$ )

## 4.2 Summary

Solar tracking algorithms that minimize radiation loss, ‘anti-tracking’ algorithms, in the field for the entire operating season can be considered an extreme case for APV systems cultivating crops requiring high irradiance levels, such as maize and other C4 crops. It should also be noted that conventionally tilted PV systems are known to affect other microclimate conditions [14]. Therefore the combined use of solar tracking and anti-tracking to optimize irradiance distribution and microclimate conditions may be most advantageous for crop growth. Further investigation is required to determine the proper anti-tracking algorithms for practical PV degrees of freedom.

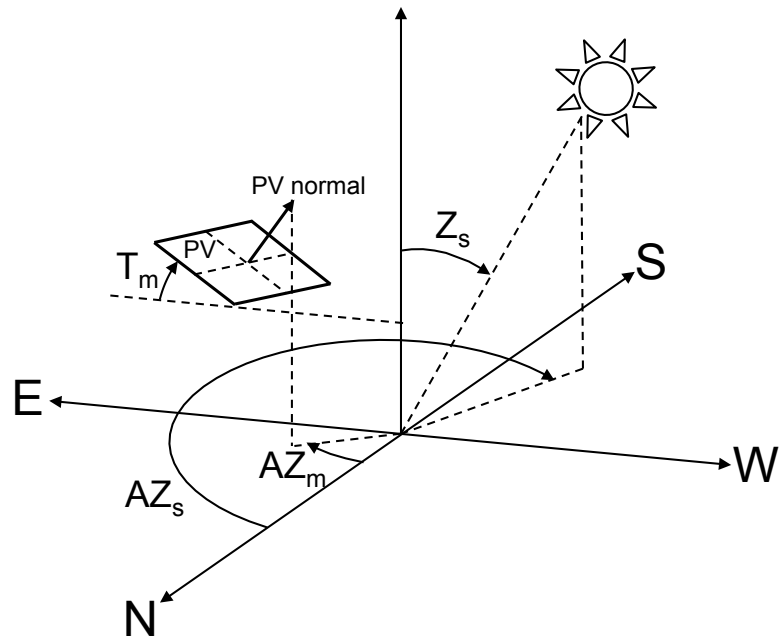


Fig. 4.1.: Coordinate system for Eqn. 4.6

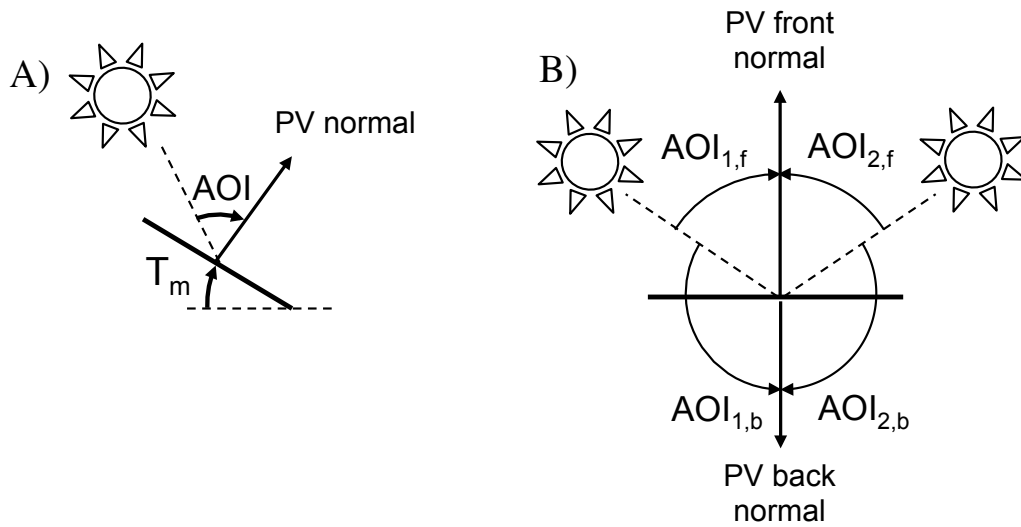


Fig. 4.2.: Definition of AOI.

## 5. SUMMARY, RECOMMENDATIONS, AND FUTURE WORK

### 5.1 Summary and Recommendations

The field of agrivoltaics is relatively young, with the first experimental agrivoltaic farm being built in France less than a decade ago [7, 13, 15]. Experimental work has been limited to early and mid-stage experimental agrivoltaic farms in France [7, 13, 15], Italy [18], and Germany [11, 12]. Modeling work has been limited and mostly from the aforementioned groups to simulate expected results from their individual agrivoltaic systems. All work, aside from work presented in this thesis, has focused on array-level modifications to traditional PV systems such as increased elevation from the ground and increased row width.

This thesis has examined and quantified relationships between agrivoltaic system output (electricity production and expected crop yield) and array-level modifications. This work has also investigated agrivoltaic designs that may improve crop yield by manipulating the duration, homogeneity, and intensity of shadows. It is found that insolation on the field can be made homogeneous by orienting PV arrays along the N-S axis. Furthermore, the relationship between panel width and spacing between panel rows has been defined for multiple tracking options, providing insight into APV system design that meets specific crop irradiance needs. Since shadow duration may affect crop yield, geometric panel patterns were explored, finding that, in a striped pattern, shadow duration is directly proportional to stripe width. Additionally, the relationship between packing fraction of the panel, ground coverage ratio, and APV system metrics is defined.

However, many concepts of potential technological benefits to the agrivoltaic field have yet to be explored. Notably, bifacial PV is a promising technology to be applied

to this niche field. Modeling of elevated bifacial PV systems in with experimentally-validated surface albedo from many commercial crops would provide an understanding of the potential of bifacial photovoltaics in an agrivoltaic context. Additionally, it is known that only a subset of the solar spectrum, photosynthetically active radiation (400 to 700 nm), is necessary for most plant photosynthesis. Researchers can take advantage of this plant characteristic to design systems that redistribute solar radiation not utilized by crops to the photovoltaic panels to increase electricity output and therefore increase the net land use efficiency of the agrivoltaic system.

The work in this thesis can and should be expanded upon to enhance our understanding of agrivoltaic systems. The dearth of experimental irradiance distribution data in agrivoltaic systems has limited our ability to experimentally validate this radiation interception model. The only experimental irradiance distribution data available is from Valle (2017), but this data provides a limited view of agrivoltaic systems as discussed in detail in Chapter 3. However, we expect more of this relevant data to be made available in time due to promising work currently being conducted by Purdue and expected growth of the agrivoltaic field.

### **5.1.1 Updates to Model**

The current model assumes the sun is a plane source. As quantified in Fig. 2.3, this introduces error that is significantly pronounced for small panel dimensions, particularly at high panel elevation from the ground. This model should be updated to reduce error introduced by the solar plane source approximation, the uniform diffuse light assumption, and the binary direct light intensity assumption. These assumptions were detailed in Chapter 2.

### **5.1.2 Bifacial PV**

Monofacial photovoltaic panels are constructed to only absorb light that is incident on the top surface typically due to an opaque back surface. Bifacial photovoltaics,

however can absorb light that is incident on both sides of the panel directly from the atmosphere and from albedo, thus increasing photovoltaic electricity production per unit area. For rooftop solar, it has been demonstrated that bifacial PV can increase electricity output by 50% by collecting albedo light [45]. It has also been simulated that globally, ground-mounted vertical bifacial farms with 2 m row spacing can produce a 10%-20% increase in electricity output compared to monofacial farms [46].

### 5.1.3 Spectrally-Selective PV Systems

Plant photosynthesis requires a subset of the solar spectrum called photosynthetically active radiation (PAR), defined as the 400-700 nm wavelength range. Solar photovoltaics, however, can utilize a greater subset of the solar spectrum. In addition to manipulating radiation intensity, there is potential to optimize the spectral component of solar radiation to meet both crop and photovoltaic needs. Spectrally selective PV that transmits the visible spectrum has been developed [47]. Electricity yield per unit area of PV compared to conventional PV will decrease because less of the spectrum is available for electricity conversion, with the theoretical limit reaching 22% [48]. However, with an ideal PV module, 100% of PAR will be transmitted, eliminating adverse effects from irradiance reduction and allowing for increased GCR (i.e. increased electricity output).

### 5.1.4 Advanced Tracking

The work in Chapter 4 demonstrates the unique potential for APV systems with effectively zero direct shadowing. In regions with low diffuse index, crops high high-irradiance needs have the potential to thrive in such APV systems. Additionally, in regions with high diffuse index, bifacial PV that can absorb a higher fraction of diffuse light than monofacial PV can offset the electricity yield loss caused by anti-tracking algorithms. In most systems, it is expected that a combination of solar tracking and anti-tracking will be employed, as demonstrated by Valle and colleagues [15].

With the rise of tracking APV systems (Tables 1.1, 1.2) further exploration into anti-tracking algorithms in combination with research into crop temporal irradiance needs may enable enhanced APV production for both food and electricity components. Additionally, research into optimal anti-tracking angles is necessary for APV systems with limited degree of freedom, such as single-axis tracking or fixed-tilt systems.

## REFERENCES

## REFERENCES

- [1] United Nations, Department of Economic and Social Affairs, Population Division. World Population Prospects: The 2017 Revision, Key Findings and Advance Tables. Working paper No. ESA/P/WP/248 (2017).
- [2] Jacobson, M. Z. et al. 100% clean and renewable wind, water, and sunlight all-sector energy roadmaps for 139 countries of the world. *Joule* 1, 108121 (2017).
- [3] C. Miskin, Y. Li, A. Perna, R. Ellis, E. K. Grubbs, P. Bermel, R. Agrawal. "Sustainable Coproduction of Food and Solar Power to Relax Land Use Constraints" *Nature Sustainability* 2019.
- [4] Ong, S., Campbell, C., Denholm, P., Margolis, R. Heath, G. Land-use requirements for solar power plants in the United States. No. NREL/TP-6A20-56290. National Renewable Energy Lab. (NREL), Golden, CO (United States).
- [5] H. Dinesh, J. M Pierce. "The potential of agrivoltaic systems" *Renewable and Sustainable Energy Reviews* 54 (2016) 299-308.
- [6] A. Goetzberger, A. Zastrow. "On the Coexistence of Solar-Energy Conversion and Plant Cultivation" *International Journal of Solar Energy* 1:1 (1982) 55-69.
- [7] C. Dupraz, H. Marrou, G. Talbot, L. Dufour, A. Nogier, Y. Ferard. "Combining solar photovoltaic panels and food crops for optimising land use: Towards new agrivoltaic schemes" *Renewable Energy* 36 (2011) 2725-2732.
- [8] United States Department of Agriculture. United States - Crop Production Maps. <https://ipad.fas.usda.gov/rssiws/al/us.cropprod.aspx>. Accessed 9 October 2019.
- [9] National Renewable Energy Laboratory. U.S. State Solar Resource Maps. <https://www.nrel.gov/gis/solar.html>. Accessed 9 October 2019.
- [10] Weselek, A., Emann, A., Zikeli, S., Lewandowski, I., Schindele, S., Hogy, P. "Agrophotovoltaic systems: applications, challenges, and opportunities. A review," *Agronomy for Sustainable Development* (2019) 39: 35 <https://doi.org/10.1007/s13593-019-0581-3>.
- [11] Fraunhofer ISE. "Harvesting the Sun for Power and Produce Agrophotovoltaics Increases the Land Use Efficiency by over 60 Percent," 2017. <https://www.ise.fraunhofer.de/en/press-media/press-releases/2017/harvesting-the-sun-for-power-and-produce-agrophotovoltaics-increases-the-land-use-efficiency.html>. Accessed 1 October 2019.
- [12] Fraunhofer ISE. "Agrophotovoltaics: High Harvesting Yield in Hot Summer of 2018," 2019. <https://www.ise.fraunhofer.de/en/press-media/press-releases/2019/agrophotovoltaics-high-harvesting-yield-in-hot-summer-of-2018.html>. Accessed 1 October 2019.

- [13] H. Marrou, J. Wery, L. Dufour, C. Dupraz. "Productivity and radiation use efficiency of luttuces grown in the partial shade of photovoltaic panels" *European Journal of Agronomy* 44 (2013) 54-66.
- [14] H. Marrou, L. Guilioni, L. Dufour, C. Dupraz, J. Wery. "Microclimate under agrivoltaic systems: Is crop growth rate affected in the partial shade of solar panels?" *Agricultural and Forest Meteorology* 177 (2013) 117-132.
- [15] B. Valle, T. Simonneau, F. Sourd, P. Pechier, P. Hamard, T. Frisson, M. Ryckwaert, A. Christophe. "Increasing the total productivity of a land by combining mobile photovoltaic panels and food crops" *Applied Energy*
- [16] Tricoles R, (2017) UA Researchers Plant Seeds to Make Renewable Energy More Efficient: Agrivoltaics, an experiment in combining agriculture with energy efficiency, involves growing plants beneath solar panels. The University of Arizona. <https://uanews.arizona.edu/story/ua-researchers-plant-seeds-make-renewable-energy-moreefficient>. Accessed 3 October, 2019.
- [17] Ravi S, Macknick J, Lobell D, Field C, Ganesan K, Jain R, Elchinger M, Stoltenberg B (2016) Colocation opportunities for large solar infrastructures and agriculture in drylands. *Appl Energy* 165:383392. <https://doi.org/10.1016/j.apenergy.2015.12.078>.
- [18] A. Amaducci, X. Yin, M. Colauzzi. "Agrivoltaic systems to optimise land use for electric energy production" *Applied Energy* 220 (2018) 545-561.
- [19] Praderio S, Perego A (2017) Photovoltaics and the agricultural landscape: the agrovoltaico concept. <http://www.remtec.energy/en/2017/08/28/photovoltaics-form-landscapes/>. Accessed 3 October, 2019.
- [20] Rem Tec (2017a) AGROVOLTAICO TECHNOLOGY. <https://www.remtec.energy/en/agrovoltaico/>. Accessed 3 October, 2019.
- [21] Corditec (2017) Our planet - Campo d'Eco. <https://corditec.it/inseguitori-solari/>. Accessed 3 October 2019.
- [22] Tonking New Energy (2018) Changshan PV station. [http://tonkingtech.com/english/news\\_show.aspx?newsCateid=117&cateid=117&NewsId=137](http://tonkingtech.com/english/news_show.aspx?newsCateid=117&cateid=117&NewsId=137) Accessed 3 October, 2019.
- [23] C. Honsberg and S. Bowden. "PV Education.ORG." (last accessed July 2019). <http://pveducation.org/pvcdrom/> (2014).
- [24] Capdevila, H., Marola, A., Herreras, M. "High Resolution Shading Modeling And Performance Simulation Of Sun-Tracking Photovoltaic Systems," *AIP Conference Proceedings* 1556, 201 (2013) <https://doi.org/10.1063/1.4822231>.
- [25] International Electrotechnical Commission. "Photovoltaic system performance monitoring-guidelines for measurement, data exchange and analysis." IEC 61724 (1998).
- [26] Reich1, N. H., Mueller, B., Armbruster, A., van Sark, W. G. J. H. M., Kiefer, K., Reise, C., "Performance ratio revisited: is PR  $\geq$  90% realistic?," *Prog. Photovolt: Res. Appl.* 2012; 20:717726

- [27] Fraunhofer Chile Research (2017b) Presentacin Proyecto FicAGRO PV Regin Metropolitana: AVANCE DE PROYECTO, March 2017
- [28] Fraunhofer Chile Research, 2017c. FIC AgroPV - FIC Region Metropolitana. [https://www.smart-agropv.com/principal/1/resultados\\_agropvr15/](https://www.smart-agropv.com/principal/1/resultados_agropvr15/). Accessed 31 May 2019.
- [29] H. Dreves. "Beneath Solar Panels, the Seeds of Opportunity Sprout." <https://www.nrel.gov/news/features/2019/beneath-solar-panels-the-seeds-of-opportunity-sprout.html>. Accessed 3 October 2019.
- [30] Perna, A., Grubbs, E.K., Agrawal, R., Bermel, P. "Design Considerations for Agrophotovoltaic Systems: Maintaining PV Area with Increased Crop Yield," /emph46<sup>th</sup> IEEE Photovoltaic Specialists Conference 2019.
- [31] Personal communication with Jeffrey J. Volenec, 2018.
- [32] Nasa POWER. <https://power.larc.nasa.gov/>. Accessed 10 October 2019.
- [33] S. Jose, Agroforestry for ecosystem services and environmental benefits: an overview. *Agroforestry systems*, vol. 76(1), pp. 1-10, 2004.
- [34] Z-P Ye. A new model for relationship between irradiance and the rate of photosynthesis in oryza sativa, *Photosynthetica*, vol. 45 (4), pp. 637-640, 2007.
- [35] Size and weight of solar panels. <https://news.energysage.com/average-solar-panel-size-weight/>. Accessed 3 October 2019.
- [36] J.S. Stein, W.F. Holmgren, J. Forbess, and C.W. Hansen. "PVLIB: Open source photovoltaic performance modeling functions for Matlab and Python." In 2016 iee 43rd photovoltaic specialists conference (PVSC), pp. 3425-3430. IEEE, 2016.
- [37] I. Stamatescu, I. Fgran, G. Stamatescu, N. Arghira, and S.S. Iliescu. "Design and Implementation of a Solar-tracking Algorithm." *Procedia Engineering* 69 (2014): 500-507.
- [38] H. Moore. *MATLAB for Engineers*. Pearson, 2017.
- [39] R. Perez, R. Seals, P. Ineichen, R. Stewart, and D. Menicucci. "A new simplified version of the Perez diffuse irradiance model for tilted surfaces." *Solar energy* 39, no. 3 (1987): 221-231.
- [40] S. Dervishi and A. Mahdavi. "Computing diffuse fraction of global horizontal solar radiation: A model comparison." *Solar Energy* 86, no. 6 (2012): 1796-1802.
- [41] J.E. Sherry and C. G. Justus. "A simple hourly all-sky solar radiation model based on meteorological parameters." *Solar Energy* 32, no. 2 (1984): 195-204.
- [42] D. Smith et al. "SunPowers Maxeon Gen III solar cell: High Efficiency and Energy Yield." *IEEE 39th Photovoltaic Specialists Conference (PVSC)* (2013).
- [43] S. Nonhebel. "Renewable energy and food supply: will there be enough land?" *Renewable and Sustainable Energy Reviews* 2005; 9 (2) 191-201.

- [44] King, D. L., Kratochvil, J. A., Boyson, W. E., “Measuring solar spectral and angle-of-incidence effects on photovoltaic modules and solar irradiance sensors,” *Sandia National Laboratories* SAND–97-1183C, CONF9-970953, 1997.
- [45] Cuevas A, Luque A, Eguren J, Del Alamo J. “50% more output power from an albedo-collecting flat panel using bifacial solar cells.” *Sol. Energy* 1982;29:41920.
- [46] M.R. Khan, A. Hanna, X. Sun, and M.A. Alam. ”Vertical bifacial solar farms: Physics, design, and global optimization.” *Applied energy* 206 (2017): 240-248.
- [47] Lunt, R. R., Bulovic, V. “Transparent, near-infrared organic photovoltaic solar cells for window and energy-scavenging applications,” *Appl. Phys. Lett.* 98, 113305 (2011); <https://doi.org/10.1063/1.3567516>.
- [48] Lunt, R.R. “Theoretical limits for visibly transparent photovoltaics,” *Appl. Phys. Lett.* 101, 043902 (2012); <https://doi.org/10.1063/1.4738896>.